https://doi.org/10.5194/acp-2019-1024
Preprint. Discussion started: 21 November 2019
© Author(s) 2019. CC BY 4.0 License.

Atmospheric Chemistry and Physics Discussions

# Impact of Urban Emissions on a Biogenic Environment during the wet season: Explicit Modeling of the Manaus Plume Organic Chemistry with GECKO-A

Camille Mouchel-Vallon[1], Julia Lee-Taylor[1,2], Alma Hodzic[1], Paulo Artaxo[3], Bernard Aumont[4], Marie Camredon[4], David Gurarie[5], Jose-Luis Jimenez[2,6], Donald H. Lenschow[7], Scot T. Martin[8,9], Janaina Nascimento[10,11], John J. Orlando[1], Brett B. Palm[2,6,a], John E. Shilling[12], Manish Shrivastava[12], and Sasha Madronich[1]

[1]Atmospheric Chemistry Observations and Modeling, National Center for Atmospheric Research, Boulder, CO 80301, USA
[2]Cooperative Institute for Research in Environmental Sciences (CIRES), University of Colorado, Boulder, CO 80309, USA
[3]University of Sao Paulo, Institute of Physics, Rua do Matao 1371, 05508-090, Sao Paulo, S.P., Brazil
[4]LISA, UMR CNRS 7583, Université Paris-Est-Créteil, Université de Paris, Institut Pierre Simon Laplace, Créteil, France
[5]Department of Mathematics and Center for Global Health and Diseases, Case Western Reserve University, Cleveland, OH 44106-7080, USA
[6]Department of Chemistry, University of Colorado, Boulder, CO 80309, USA
[7]Mesoscale and Microscale Meteorology Laboratory, National Center for Atmospheric Research, Boulder, CO 80301, USA
[8]School of Engineering and Applied Sciences, Harvard University, Cambridge, MA 02318, USA
[9]Department of Earth and Planetary Sciences, Harvard University, Cambridge, MA 02318, USA
[10]Post-graduate Program in Climate and Environment, National Institute for Amazonian Research and Amazonas State University, Manaus, AM, Brazil
[11]Chemical Sciences Division, NOAA Earth System Research Laboratory, Boulder, CO 80305, USA
[12]Pacific Northwest National Laboratory, Richland, WA 99352, USA
[a]Now at Department of Atmospheric Sciences, University of Washington, Seattle, WA 91895, USA

**Correspondence:** C. Mouchel-Vallon (cmv@ucar.edu)

**Abstract.** The GoAmazon 2014/5 field campaign took place in Manaus (Brazil) and allowed the investigation the interaction between background level biogenic air masses and anthropogenic plumes. We present in this work a box model built to simulate the impact of urban chemistry on biogenic Secondary Organic Aerosol (SOA) formation and composition. An organic chemistry mechanism is generated with the Generator for Chemistry and Kinetics of Organics in the Atmosphere (GECKO-A) to simulate the explicit oxidation of biogenic and anthropogenic compounds. A parameterization is also included to account for the reactive uptake of isoprene oxidation products on aqueous particles. After some reductions of biogenic emissions relative to existing emission inventories, the model is able to reproduce measured primary compounds, ozone and NOx for clean or polluted situations. The explicit model is able to reproduce background case SOA mass concentrations but is underestimating the enhancement observed in the urban plume. Oxidation of biogenic compounds is the major contributor to SOA mass. A Volatility Basis Set parameterization (VBS) applied to the same cases obtains better results than GECKO-A for predicting SOA mass in the box model. The explicit mechanism may be missing SOA formation processes related to the oxidation of monoterpenes that could be implicitly accounted for in the VBS parameterization.

https://doi.org/10.5194/acp-2019-1024
Preprint. Discussion started: 21 November 2019
© Author(s) 2019. CC BY 4.0 License.



## 1 Introduction

The Amazonian rainforest is the largest emitter of biogenic primary hydrocarbons on Earth (*e.g.* Guenther et al., 2012). Photochemistry in this tropical region is particularly intense all year long, which stimulates the oxidation of the biogenic primary compounds by oxidants such as ozone and OH radicals. This part of the world is consequently a substantial source of Secondary Organic Aerosol (SOA) (Martin et al., 2010; Chen et al., 2015a) produced by condensation of oxygenated secondary organic species formed from gas and aqueous phase oxidation of biogenic compounds (Claeys, 2004; Carlton et al., 2009; Paulot et al., 2009). On the other hand, the city of Manaus (Brazil) is a source of anthropogenic pollution with 2.1 million inhabitants, ca. 600000 vehicles in circulation and 78 thermal power plants in its close surroundings (Abou Rafee et al., 2017). Manaus is situated at the confluence of the Rio Negro and Solimões rivers that subsequently form the Amazon River (Fig. 1). This metropolis is isolated from the rest of South American populated areas by over 1000 km of Amazonian tropical rainforest in every direction (*e.g.* Martin et al., 2016). Manaus is therefore a point source of urban pollution in a vast rainforest, making it an ideal place to study chemical interactions of biogenic and anthropogenic compounds. The Observations and Modeling of the Green Ocean Amazon (GoAmazon 2014/5) experiment was designed to characterize the anthropogenic perturbations to the clean air masses influenced by Amazonian natural emissions (Martin et al., 2016). The main instrumented site (T3) was situated approx. 70 km southwest of Manaus (see Fig. 1). In addition, the US Department of Energy (DOE) Gulfstream research aircraft (G-1) conducted 16 research flights to sample the Manaus plume as it was transported downwind and over the Amazon forest (Martin et al., 2016; Shilling et al., 2018). With varying meteorological conditions, this allowed sampling of clean background air from the Amazon basin and polluted air from Manaus (Martin et al., 2016).

Several studies have already shown that the overall composition of particulate matter (PM) in remote areas is distinctly different from urban areas, with anthropogenic PM being characterized by more sulfates and hydrocarbon-like compounds, whereas remote PM contains more oxidized organic matter (e.g. Xu et al., 2015; Budisulistiorini et al., 2016). In the Manaus environment, biogenic molecules would interact with the chemistry resulting from anthropogenic emissions. de Sá et al. (2018) have shown that the majority of sub micrometer particle mass at the T3 site is secondary. Would SOA retain their biogenic nature and how would they exhibit anthropogenic influence? For instance Aerosol Mass Spectrometer (AMS) measurements reported by de Sá et al. (2017) have shown that the contribution of epoxydiols derived from isoprene to SOA (IEPOX-SOA) amounts to 11 to 17% of the total organic mass when the Manaus plume is sampled, compared to 19 to 26% under background conditions. Using an Oxidation Flow reactor (OFR) and tracers for different source types, Palm et al. (2018) concluded that the Volatile Organic Compounds (VOC) and Intermediate Volatility Organic Compounds (IVOC) sampled during GoAmazon2014/5 could form SOA whose origin would be dominated by biogenic sources during the dry season, and by both biogenic and anthropogenic sources during the wet season. With a regional model study of the GoAmazon 2014/5 situation, Shrivastava et al. (2019) concluded that the higher oxidative capacity in the urban plume results in an enhancement of biogenic SOA production.

Models need to take into account the different nature of VOCs and SOA resulting from biogenic and anthropogenic chemistry to accurately represent their interactions. This can be done by looking at this problem with what Pankow et al. (2015) call

https://doi.org/10.5194/acp-2019-1024
Preprint. Discussion started: 21 November 2019
© Author(s) 2019. CC BY 4.0 License.

Atmospheric Chemistry and Physics Discussions

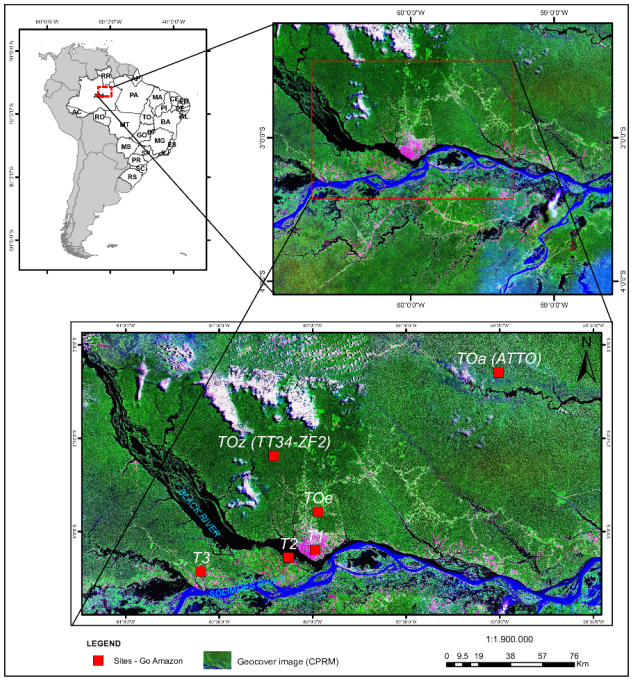


**Figure 1.** Map of the GoAmazon field campaign instrumented sites. Measurements used in this work came from the T3 site. Source: GeoCover, Instituto Brasileiro de Geografia e Estatistica (IBGE).

a "molecular view", as opposed to the "anonymized view" followed by current 3D models. The molecular view attempts to predict SOA mass from the known and estimated properties of individually simulated organic compounds while the anonymized view uses hypothetical properties (*e.g.* volatility, solubility) of a small number of lumped compounds. Even though a few instruments are getting closer to providing this molecular view of volatile organic compounds (e.g. Koss et al., 2017a, b), such measurements are not available for the GoAmazon 2014/5 campaign. 3D models that were run for the Manaus situation offer an anonymized view of SOA composition (Shrivastava et al., 2019) because they rely on a Volatility Basis Set parameterization (VBS, Donahue et al., 2006). The Generator for Explicit Chemistry and Kinetics of Organics in the Atmosphere (GECKO-A, Aumont et al., 2005; Camredon et al., 2007) is the ideal tool to model atmospheric organic chemistry with a detailed molecular view. GECKO-A is an automated chemical mechanism generator built to write the explicit chemistry of given precursors by following a prescribed set of systematic rules. This set of systematic rules relies on experimental data when available and Structure Activity Relationships (SAR) to determine unknown kinetic or thermodynamic constants. It has previously been run in box models to evaluate processes like secondary organic aerosol formation (Valorso et al., 2011; Aumont et al., 2012; Camredon and Aumont, 2006; Camredon et al., 2007) and dissolution of organic compounds (Mouchel-Vallon et al., 2013). It was also applied to simulate chamber experiments (Valorso et al., 2011; La et al., 2016) and urban and biogenic plumes (Lee-Taylor et al., 2011, 2015).

https://doi.org/10.5194/acp-2019-1024
Preprint. Discussion started: 21 November 2019
© Author(s) 2019. CC BY 4.0 License.



In this work, a box model is run to simulate the evolution of an Amazonian air mass intercepting Manaus emissions during the wet season. Emissions of anthropogenic and biogenic primary VOCs are estimated with available data. The chemical scheme describing the explicit oxidation of these primary compounds is generated with GECKO-A. The resulting detailed simulation is then used to explore the impact of Manaus emissions on the Amazonian biogenic chemistry. Comparisons with aerosol mass spectrometer data and the VBS parameterization are carried out to identify important processes involved in biogenic SOA formation that may not be accounted for in GECKO-A. Finally the potential for reduction of the explicit mechanism is estimated.

## 2 Experimental Data

The main instrumented site (referred to as T3 hereafter) of the GoAmazon 2014/5 field campaign was situated 70 km west of Manaus (Fig. 1). Two aircraft were also deployed, a G-159 Gulfstream I (G-I) (Schmid et al., 2014) that flew at low altitude and mostly sampled the boundary layer and a Gulfstream G550 (HALO) that flew higher altitudes and sampled the free troposphere (Wendisch et al., 2016). The flight tracks are depicted in Martin et al. (2016) and Wendisch et al. (2016). The G-1 airplane mainly flew daytime transects of the Manaus plume between the city and the T3 site.

The detailed instrumentation deployed at T3 and in the airplanes has been described elsewhere (Martin et al., 2016). For this study we mainly relied on ground deployed instruments briefly described here.

Ozone concentration measurements made with a Thermo Fisher Model 49i Ozone Analyzer were obtained from the Mobile Aerosol Observing System-Chemistry (MAOS-C).

Due to some issues with the $NO_x$ analyzer deployed at T3 by the MAOS-C during the wet season, $NO_x$ data reported here is weakly reliable. The values reported here are only qualitative indications of $NO_x$ levels in the studied period.

OH radicals concentrations were provided by an OH chemical ionization mass spectrometer (Sinha et al., 2008, OH-CIMS).

Organic compounds in the gas phase were measured with selected reagent ion proton transfer reaction time-of-flight mass spectrometer (SRI-PTR-ToFMS, Jordan et al., 2009a, b). Aerosol composition was monitored by a high-resolution time-of-flight aerosol mass spectrometer (HR-ToF-AMS) (DeCarlo et al., 2006; de Sá et al., 2018, 2019).

For the purpose of comparisons with the model, we need to be able to separate time periods representing clean and polluted episodes. Using a fuzzy c-means clustering algorithm (Bezdek, 1981; Bezdek et al., 1984) applied to T3 measurements, de Sá et al. (2018) were able to identify four different clusters corresponding to (i) fresh or (ii) aged (2+ days) biogenic production, and air masses influenced by the (iii) northern or (iv) southern parts of Manaus. Using the timeseries contribution of these clusters, we labeled as background air masses that were identified as being composed of at least 50% of any clean cluster (i or ii). Conversely, air masses that were identified by de Sá et al. (2018) as being composed of at least 50% of any polluted cluster (iii and iv) were labeled as polluted. The clustering methods constrained the classification to only include wet season afternoon air masses that were not exposed to rain in the previous day (see de Sá et al., 2018). These limitations match with our model restrictions which do not include cloud chemistry, nor fire emissions that would be important during the dry season. For comparison with the model, experimental data were hourly averaged for each cluster.

https://doi.org/10.5194/acp-2019-1024
Preprint. Discussion started: 21 November 2019
© Author(s) 2019. CC BY 4.0 License.



**Table 1.** Box model constraints used in the clean and polluted setups

| | Clean Background | Manaus |
|---|---|---|
| NO soil emission [molec $cm^{-2}$ $s^{-1}$][(a)] | $8.3\times10^{9}$ | – |
| Aerosol number concentration [$cm^{-3}$][(b)] | $5\times10^{2}$ | $1\times10^{4}$ |
| Aerosol pH | 3.0 | 1.5 |
| Aerosol sulfate concentration [μg $m^{-3}$][(b)] | 0.3 | 0.4 |
| Aerosol nitrate concentration [μg $m^{-3}$][(b)] | 0.05 | 0.1 |
| Hygroscopicity Parameter ($\kappa$)[(c)] | 0.15 | 0.15 |

[(a)]Shrivastava et al. (2019) [(b)]de Sá et al. (2018) [(c)]Thalman et al. (2017)

## 3 Model Setup

A Lagrangian box model was built to simulate chemistry in the planetary boundary layer and the residual layer for an air parcel traveling over the Amazonian forest and Manaus. Because experimental data compared to the model only contain air masses that were not exposed to rain in the previous day (see Sect. 2 and de Sá et al., 2018), the model simulates biogenic conditions for one day, assuming the air mass was washed out by rain prior to that day. After the one day spinup, biogenic emissions are replaced by urban emissions for one hour during the second day to represent the interaction of the air mass with the Manaus urban area. After the simulated encounter with Manaus, the model inputs return to biogenic emissions until the end of the second day. This simulation is defined hereafter as the "polluted" case. Another simulation is run where the box is only subjected to biogenic emissions for two days, without any exposure to urban emissions to simulate a background case. This simulation is defined hereafter as the "clean" case. This section describes the box model setup, how the emissions were defined and the chemical mechanism used for this study.

### 3.1 Box model

This study relies on a box model described in this section. It includes emissions from the forest and the city, deposition and chemical evolution of the trace gases. Daytime growth of the planetary boundary layer is also simulated, with mixing with the residual layer.

#### 3.1.1 Boundary Layer

The model includes two boxes on top of each other separated by a moving boundary representing the height of the boundary layer. The bottom box extends from the surface to the top of the planetary boundary layer (PBL). The top box extends from the top of the planetary boundary layer to 1.5 km and represents the residual layer (RL) (see Fig. 2). The daytime PBL height evolution is parameterized according to the Tennekes (1973) approach and was calculated using the Second-Order Model for Conserved and Reactive Unsteady Scalars (SOMCRUS, Lenschow et al., 2016) (see Fig. 2). At sunset, stratification is assumed

https://doi.org/10.5194/acp-2019-1024
Preprint. Discussion started: 21 November 2019
© Author(s) 2019. CC BY 4.0 License.



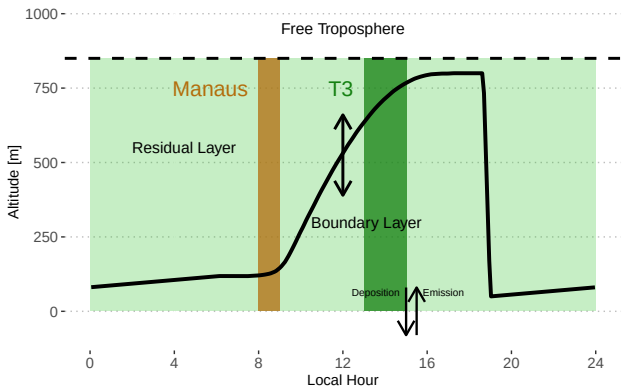


**Figure 2.** Schematic depiction of the box model setup used in this work. The continuous black line shows the time evolution of the PBL height. The dashed black line depicts the top of the residual layer box. The brown shaded area is the period when the box is subjected to Manaus emissions. For the rest of the time period, the box is subjected to biogenic emissions (light and dark green shaded areas). The dark green shaded area is approximately the period when the box would be over the main instrumented site T3, assuming a travel time of 4 to 6 hours.

to quickly shrink the PBL to 50 m which results in the contents of the PBL being reallocated to the RL. During the night, the PBL is constrained to linearly grow to reach the next morning level. The PBL height evolution is the same for each of the two simulated days. During the day, the PBL is therefore slowly incorporating residual chemicals resulting from the previous day and night chemistry. Thalman et al. (2017) report PBL heights estimated from ceilometer measurements during the wet season in the central Amazonian Forest, for polluted and background conditions. The measurements reach a maximum of 800 m at around 3pm local time. This value was used to further constrain the PBL height evolution by scaling the SOMCRUS output to reach this measured PBL height maximum. The growth and shrinking of the PBL dilute the expanding box and transfer gases from the shrinking box to the expanding box. This is parameterized according to Eqs. 1 and 2:

$$\frac{dC_b}{dt} = \begin{cases} \frac{1}{h}\frac{dh}{dt}C_t - \frac{1}{h}\frac{dh}{dt}C_b & \text{if } \frac{dh}{dt} > 0 \\ 0 & \text{if } \frac{dh}{dt} \leq 0 \end{cases} \tag{1}$$

$$\frac{dC_t}{dt} = \begin{cases} 0 & \text{if } \frac{dh}{dt} \geq 0 \\ -\frac{1}{H-h}\frac{dh}{dt}C_b + \frac{1}{H-h}\frac{dh}{dt}C_t & \text{if } \frac{dh}{dt} < 0 \end{cases} \tag{2}$$

$C_b$ and $C_t$ [molec cm$^{-3}$] are chemical species concentrations in the PBL (bottom) and RL (top) boxes respectively. $h$ [m] is the variable height of the PBL and $H$ [m] is the fixed altitude of the RL top. The first term in each equation describes the addition of material coming from the shrinking box and the second term describes the dilution of the growing box. Following these equations, mixing happens in two stages: (i) the long RL entrainment into the PBL over day time and (ii) the rapid transfer of the PBL to the RL at sunset. The box model approach assumes rapid mixing in both layers and that chemistry is applied to

https://doi.org/10.5194/acp-2019-1024
Preprint. Discussion started: 21 November 2019
© Author(s) 2019. CC BY 4.0 License.



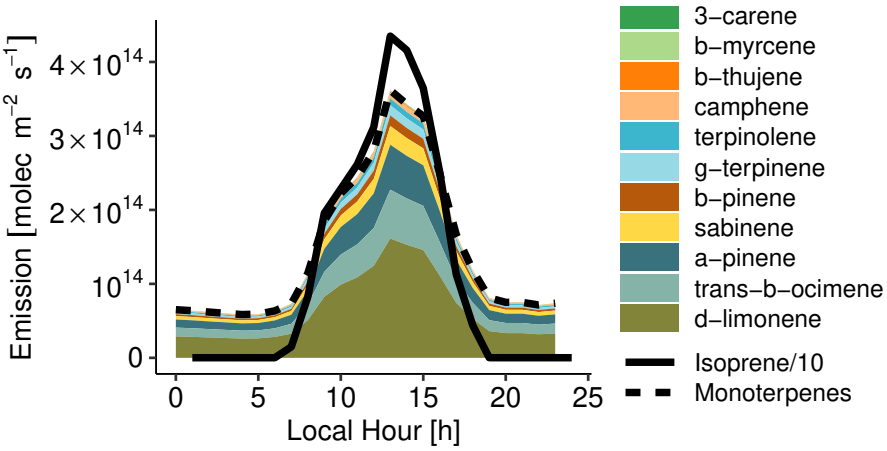


**Figure 3.** Hourly biogenic emissions estimated with MEGAN and scaled to match measured concentrations (see 3.2.1). The lines depict isoprene (continuous line) and total monoterpenes (dashed line). The colored areas depict the contribution of each individual species to total monoterpenes. Please note that isoprene emissions are divided by 10 to fit on the plot.

well-mixed concentrations. The residual layer is also slowly mixed with the free troposphere. The free troposphere is assumed to be a fixed reservoir of CO (80 ppb) and ozone (15 ppb, *e.g.* Browell et al., 1990; Gregory et al., 1990; Kirchhoff et al., 1990). The subsidence velocity is constant and fixed at 0.1 m s$^{-1}$ (*e.g.* Raes, 1995).

Temperature is assumed to follow a sinusoidal daily variation, with an average of 27 °C, an amplitude of 4 °C and a maximum at 6 pm local time. Relative humidity is initially set at 75% at 6 am (23 °C) and is free to evolve with temperature changes assuming water vapor concentration is constant.

## 3.2 Emissions

### 3.2.1 Biogenic Emissions

VOC emissions from the rainforest were estimated with the Model of Emissions of Gases and Aerosols from Nature (MEGAN v2.1, Guenther et al., 2012). Biogenic emissions on March, 13$^{th}$ 2014 (the golden day of the GoAmazon field campaign, see de Sá et al., 2017) in a domain situated in the forest around Manaus were averaged to obtain total isoprene and monoterpene hourly averaged emissions for a day typical of the wet season, without any recorded rain event. Monoterpenes were then speciated to match concentrations measured by Jardine et al. (2015) at the top of an Amazonian rainforest canopy. Based on this emission inventory, we then simultaneously optimized isoprene and monoterpenes emissions to match the model with T3 isoprene and total monoterpenes under clean conditions. This resulted in the need to reduce isoprene emissions by a factor of 7. Using measurements from a similar site in Amazonia, Alves et al. (2016) reported that MEGAN 2.1 overestimated isoprene emissions by a factor of 5 on average during the dry season. They assumed that the T3 site configuration (a clearing in the forest, near a road) could affect local isoprene concentrations compared to average Amazonian emissions. For instance measurements

https://doi.org/10.5194/acp-2019-1024
Preprint. Discussion started: 21 November 2019
© Author(s) 2019. CC BY 4.0 License.

Atmospheric Chemistry and Physics Discussions

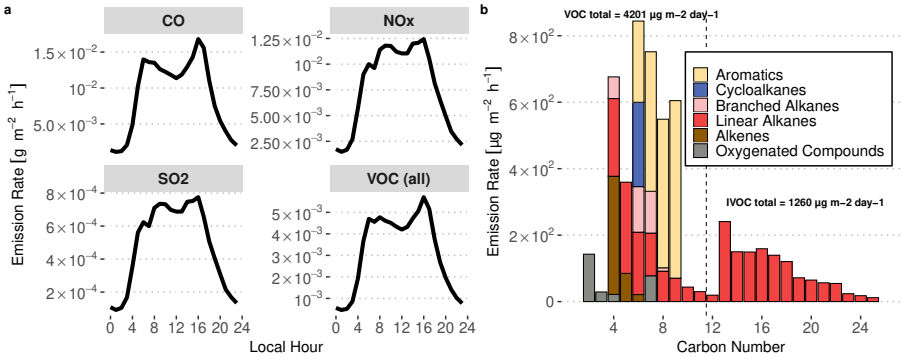


**Figure 4.** Diurnal evolution of simulated traffic emissions in Manaus deduced from inventories in Manaus and Saõ Paulo. (a) $NO_x$, $SO_2$, CO and total VOC daily emissions. (b) Carbon number distribution of Manaus emissions at noon. Total daily emissions are indicated for lighter organic compounds (VOC) and less volatile compounds (IVOC). The dashed line denotes the separation between VOCs (left) and IVOCs (right).

in the Amazon rainforest by Batista et al. (2019) indicate that biogenic emissions exhibit large intermediate scale heterogeneity, with estimated emission variations of 220% to 330%. Recent satellite based estimates of biogenic emissions also reported that MEGAN overestimates isoprene emissions in Amazonia by 40% (Worden et al., 2019). In a similar way, monoterpenes emissions had to be reduced by a factor of 8 compared to the MEGAN values. Figure 3 depicts the resulting daily biogenic emission cycle. Isoprene emissions dominate monoterpene emissions by approximately an order of magnitude. $\delta$-limonene is the most emitted monoterpene (45%), followed by trans-$\beta$-ocimene (18%) and $\alpha$-pinene (17%). NO soil emissions are also accounted for with a constant flux of $8.3\times10^{9}$ $\mathrm{molec\,cm^{-2}\,s^{-1}}$ following Shrivastava et al. (2019).

### 3.2.2 Manaus Emissions

The emissions used to represent the influence of Manaus are shown in Fig. 4a and were calculated following the methodology described in Abou Rafee et al. (2017). Traffic emissions have been estimated from vehicle use intensity and emission factors for CO, $NO_x$, $SO_2$ and VOCs depending on type of fuel use in Manaus (Abou Rafee et al., 2017). VOC speciation is assumed to be similar to the average speciation of the vehicle fleet emissions of São Paulo, Brazil in 2004 (Martins et al., 2006). Hourly distribution of the traffic emissions is considered to be similar to the hourly traffic distribution in São Paulo (Andrade et al., 2015). In the past decades, Brazil has become known for pioneering the large scale use of ethanol based biofuels. However, due to its isolation and being distant from south Brazilian biofuel producing regions, Manaus traffic doesn't involve consumption of significant amounts of ethanol-based fuel.

This emission estimate does not include Intermediate Volatile Organic Compounds (IVOC) which would mainly be produced by diesel vehicle emissions (Gentner et al., 2012, 2017). Zhao et al. (2015, 2016) showed that the IVOC to VOC emissions ratio lies between 4% for gasoline vehicles and 65% for diesel vehicles. Knowing that diesel vehicles account for ca. 45% of the total driven distance in Manaus (Abou Rafee et al., 2017), we therefore assume that IVOC total emissions are approximately

https://doi.org/10.5194/acp-2019-1024
Preprint. Discussion started: 21 November 2019
© Author(s) 2019. CC BY 4.0 License.



equal to 30% of total VOC emissions. To estimate the distribution of species resulting from IVOC emissions, we assumed that the distribution in volatility is similar to the distribution used to simulate traffic emissions in Mexico City in Lee-Taylor et al. (2011), with n-alkanes from $C_{12}$ to $C_{25}$ acting as surrogates for these heavier emitted organic compounds.

The resulting distribution of urban organic emissions at noon as a function of the number of carbon atoms is presented in Fig. 4b. As reported in the Gentner et al. (2017) review, gasoline emissions have a maximum for $C_8$ species, with no emission of importance above $C_{12}$, whereas diesel vehicles emit species from $C_{10}$ to $C_{25}$, with a peak at $C_{12}$. These features are present in the emissions estimated in this work, with the gasoline peak around $C_{6\text{-}7}$ and the diesel maximum at $C_{13}$. Gentner et al. (2017) also report that half of the gasoline VOC emissions are composed of linear and branched alkanes, the other half consisting of aromatics and cycloalkanes. In our estimates of gasoline emissions ($C_{<12}$) the proportion of branched alkanes is smaller, alkenes constitute a more important fraction of emitted $C_{4\text{-}6}$ species, branched cycloalkanes are missing, and aromatics constitute the majority of emissions of $C_{7\text{-}10}$ compounds. These differences could represent differing sources of fuels or different distributions of vehicle brands and ages. In the case of diesel emissions, Gentner et al. (2017) report that they are approximately equally distributed between aromatics, branched cycloalkanes, bicycloalkanes and branched alkanes whereas our method leads to diesel emissions being only constituted of n-alkanes, which are used here as surrogate species for the entire mixture.

### 3.3 Chemical Mechanism

#### 3.3.1 GECKO-A

All emitted organic compounds were used as inputs to GECKO-A to automatically generate the chemical scheme used in this study. The GECKO-A protocol has been described in detail in Aumont et al. (2005) and updated in Camredon et al. (2007), Valorso et al. (2011), Aumont et al. (2013), and La et al. (2016). Partitioning of low volatility compounds to the aerosol phase is described dynamically as in La et al. (2016). Vapor pressures are estimated with the Nannoolal et al. (2008) structure activity relationship. As isoprene first oxidations steps have been widely studied in the literature, there is no need to automatically generate them with GECKO-A. Isoprene chemistry first two generations of oxidation were therefore taken from the Master Chemical Mechanism 3.3.1 (Jenkin et al., 1997; Saunders et al., 2003; Jenkin et al., 2015, MCM, *e.g.*). With 12 biogenic and 53 anthropogenic precursors ranging from $C_2$ to $C_{25}$, some reductions are carried out to reduce the size of the generated mechanisms. Species with an estimated vapor pressure below $10^{-13}$ atm are assumed to entirely partition to the aerosol phase so quickly that a description of their gas phase oxidation is not needed (Valorso et al., 2011). Furthermore, lower yield, longer chain species are lumped with chemically similar compounds according to a a hierarchical decision tree based on molecular structure (Valorso et al., 2011). The resulting chemical scheme contains 16 million reactions involving 4 million species of which 470000 can partition into the aerosol phase. The time integration in the two-box model setup takes approximately 0.5 computing hour per simulated hour on 16 cores (Computational and Information Systems Laboratory, 2017).

https://doi.org/10.5194/acp-2019-1024
Preprint. Discussion started: 21 November 2019
© Author(s) 2019. CC BY 4.0 License.



### 3.3.2 Isoprene SOA formation

GECKO-A treats SOA formation through a dynamic approach that converges towards the equilibrium defined by the Pankow formulation of Raoult's Law (Pankow, 1994). However it is likely that isoprene SOA (ISOPSOA) formation is not only controlled by vapor pressure (Paulot et al., 2009). Among factors that have been identified to play a role in ISOPSOA are: aqueous phase oxidation in deliquescent aerosol (*e.g.* Blando and Turpin, 2000; Ervens et al., 2011; Daumit et al., 2016), organic sulfate/nitrate formation via interaction with the inorganic component of the aerosol (*e.g.* McNeill et al., 2012; Pratt et al., 2013; Wang et al., 2018; Glasius et al., 2018; Jo et al., 2019), and accretion reactions in the bulk aerosol (*e.g.* oligomerization, dimerization, Altieri et al., 2006; Liu et al., 2012; Renard et al., 2015). None of these processes is currently implemented in the GECKO-A framework. For this study we use a simplified approach based on Marais et al. (2016) allowing the representation of ISOPSOA formation depending on the assumed composition of the inorganic aerosol. This parameterization describes the heterogeneous reactive uptake of important isoprene oxidation products. This accounts for the diffusion of the gases to the surface of the wet aerosol particle, their accomodation to the surface and their dissolution. The relevant parameters used here are listed in Marais et al. (2016). Isoprene epoxides (epoxydiols and hydroxyepoxides) react in the aqueous phase to open their epoxide ring via acid-catalized reactions. These reactions are followed by either the nucleophilic addition of (i) $H_2O$ to form methyltetrols or (ii) sulfate and nitrate ions to form organosulfates and organonitrates. The uptake of epoxides therefore depends on the acidity of particles, as well as their sulfate and nitrate content. These parameters had to be constrained in the model and were deduced from the T3 AMS measurements and literature data (see Table 1). On the other hand, isoprene oxidation products containing nitrate moieties (dihydroxydinitrates and isoprene nitrate) hydrolyze and form polyols and nitric acid.

### 3.4 Dry Deposition

Dry deposition is treated following the Wesely (1989) parameterization. This parameterization is a resistance model that allows calculating dry deposition velocities based on multiple resistances defined as properties of the surfaces. The city and the forest were respectively attributed the properties of surfaces defined as urban and deciduous forest in the Wesely (1989) paper. The dry deposition velocity of a given species depends on its solubility expressed by its Henry's law coefficient. Because the solubility of most organic compounds generated with GECKO-A is unknown, they are here estimated using the GROupcontribution Method for Henry's law Estimate SAR (Raventos-Duran et al., 2010).

## 4 Results and Discussion

### 4.1 Gas Phase Organics: Primary Organic Compounds and Oxidants

Figure 5 depicts the time evolution of selected primary organic species, and compares the model with available measurements. In the clean situations, measured isoprene mixing ratios range from 2–3 ppb at noon to 5–6 ppb at the end of the afternoon. The sum of all monoterpenes follows a similar increasing trend in the afternoon, from 0.1 to 0.3 ppb. After adjusting biogenic

https://doi.org/10.5194/acp-2019-1024
Preprint. Discussion started: 21 November 2019
© Author(s) 2019. CC BY 4.0 License.

Atmospheric Chemistry and Physics Discussions

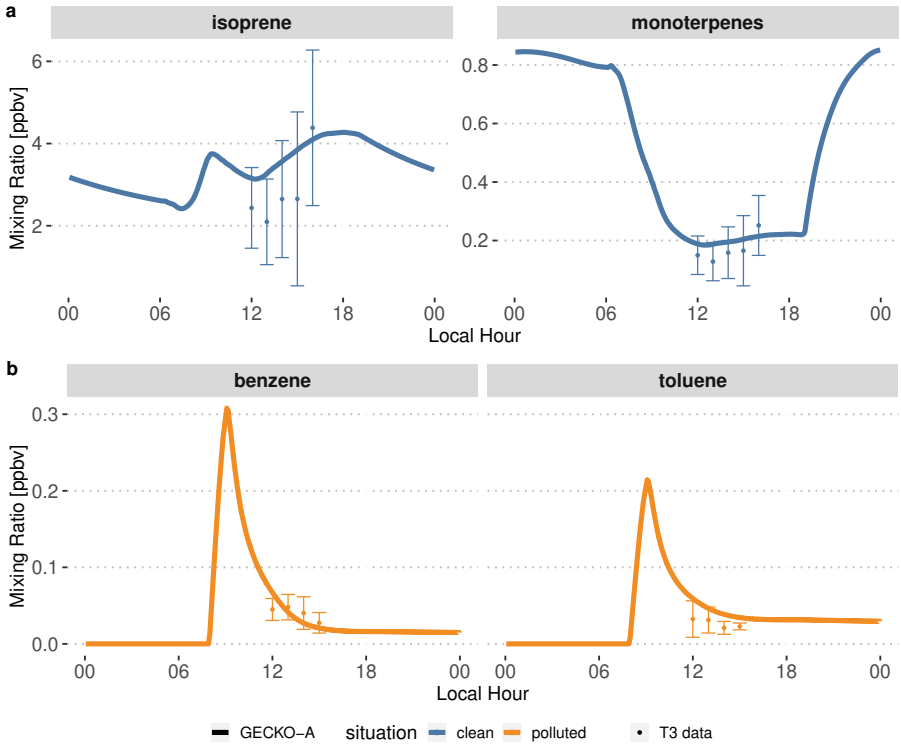


**Figure 5.** Modeled (lines, second day) time evolution of primary species concentrations in the Lagrangian box-model described in Sect. 3.1 and average experimental (dots) concentrations measured at the T3 site. The vertical range of the experimental data denotes the standard deviation of measured concentrations during events identified as clean (top, blue) and polluted (bottom, orange).

emissions rates (see Sect. 3.2.1), the model is able to reproduce these mixing ratios, with isoprene and monoterpenes being simulated in the higher range of experimental values. In polluted situations, the model shows a peak of anthropogenic organic compounds when the plume encounters Manaus emissions between 8 and 9 am. This peak reaches 0.3 ppb and 0.2 ppb respectively for benzene and toluene (Fig. 5). Their levels decay for the remainder of the day. Because the T3 measurement site is situated 4 to 6 hours downwind of Manaus, measurements of benzene and toluene can be compared to decayed modeled levels after that time span. The modeled mixing ratio of benzene matches the lower range of measurements, between 0.2 and 0.6 ppb, while modeled toluene is closer to the higher range of measurements, between 0.4 and 0.6 ppb during the afternoon.

Pristine forest conditions are characterized in the model by low $NO_x$ emissions from the soil ($8.3 \times 10^9$ molec cm$^{-2}$ s$^{-1}$ $\approx$ $1.5 \times 10^{-5}$g m$^{-2}$ h$^{-1}$, see Table 1). The model predicts $NO_x$ mixing ratios around 50 ppt in the afternoon. In the polluted case, the background air mass is exposed to a complex mixture of anthropogenic compounds emissions as well as three orders of magnitude higher $NO_x$ emissions ($\approx 1 \times 10^{-2}$g m$^{-2}$ h$^{-1}$, see Fig. 4). This leads to modeled $NO_x$ between 500 ppt and 2 ppb in the afternoon, after a 25 ppb peak in the city in the morning. The increase in $NO_x$ is not as important in the experimental data, but these $NO_x$ measurements are highly uncertain, which could explain the modeled discrepancies.

https://doi.org/10.5194/acp-2019-1024
Preprint. Discussion started: 21 November 2019
© Author(s) 2019. CC BY 4.0 License.



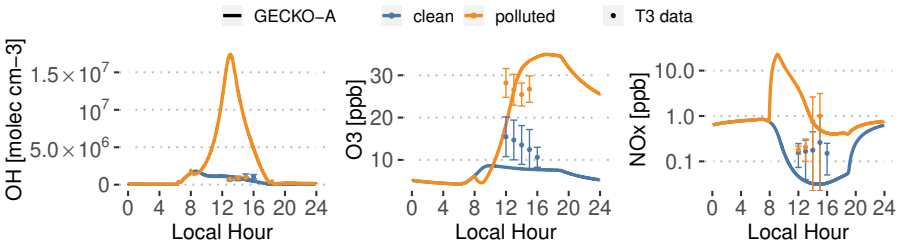


**Figure 6.** Experimental (dots, T3 site) and modeled (lines, second day) time evolution of OH radicals concentrations (left), ozone (middle) and $NO_x$ (right, note log scale) mixing ratios. The vertical range of the experimental data denotes the standard deviation of measured concentrations at T3 during events identified as clean (blue) and polluted (orange).

Modeled daytime ozone mixing ratios of 7 to 8 ppb in the clean situation, in the lower range of measured values. The higher $NO_x$ levels result in strong ozone production in the polluted plume, characterized by mixing ratios of 16 ppb at noon and up to 33 ppb at the end of the afternoon. These values are in the upper range of measured ozone at T3 during polluted events. On average, measured ozone in the polluted case is a factor of 2 higher than the clean case while the model sees an increase by a factor of more than 3. It should also be noticed that the model completely separates clean and polluted situation, which increases the contrast for all variables compared to the classification of the measurements that always includes some degree of mixing (see 2). The nighttime decay of ozone can be explained by dry deposition to the forest surface.

Furthermore, VOCs in the plume are exposed to high OH concentrations, with modeled concentration reaching $1.6\times10^7$ molec cm$^{-3}$ in the afternoon. In the clean background, OH concentrations only reach $1\times10^6$ molec cm$^{-3}$. These clean values are in the lower range of reported measurements at T3. Unlike the model, OH measurements averaged at T3 and identified as clean and polluted did not exhibit any difference between both situations. (Fig. 6). In that case, there could be issues with the OH measurements at T3. Indirect constraints have shown differences between clean and polluted situations. Liu et al. (2018) derived OH concentrations from isoprene and its oxidation products measurement. They showed that noontime OH concentrations vary between $5\times10^5$ molec cm$^{-3}$ in clean situations to $1.5\times10^6$ molec cm$^{-3}$ in polluted events. The Shrivastava et al. (2019) 3D model exhibits a similar OH behavior to this work with concentrations at T3 ranging from $2\sim5\times10^5$ molec cm$^{-3}$ (clean) to more than $4\times10^6$ molec cm$^{-3}$ (polluted). The GECKO-A model is therefore likely to be overestimating OH concentrations in the urban plume by a factor of 5 to 10. This could stem from either overestimating NO or underestimating VOCs emissions in the city.

### 4.2 Modeled Urban Impact on SOA Mass and Composition

#### 4.2.1 Modeled vs Measured SOA Mass Concentrations

At the measurement site, SOA mass concentrations measured by AMS range from 0.6 to 2.5 µg m$^{-3}$ in clean conditions. In polluted conditions, SOA mass concentrations range from 1.9 to 2.9 µg m$^{-3}$ (Fig. 7). In the clean case, the modeled SOA mass is within the lower range of T3 measurements, increasing from 0.2 µg m$^{-3}$ at sunrise to 1.25 µg m$^{-3}$ at the end of the

https://doi.org/10.5194/acp-2019-1024
Preprint. Discussion started: 21 November 2019
© Author(s) 2019. CC BY 4.0 License.



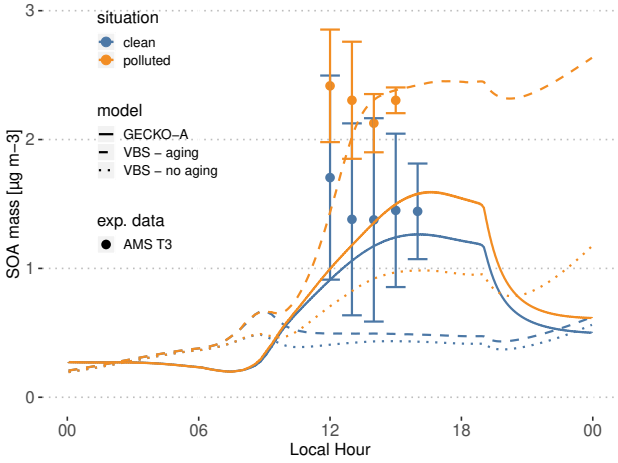


**Figure 7.** Experimental (circles, T3 site) and modeled (lines, second day) time evolution of SOA mass concentration. The vertical range of the experimental data denotes the standard deviation of measured concentrations. Cases are identified as clean (blue) and polluted (orange). The continuous lines depict the GECKO-A model run and the dashed lines depict the modeled SOA mass predicted with the VBS approach from Shrivastava et al. (2019). The dotted lines depict modeled SOA mass predicted with the VBS approach without including aging processes (see Sect. 4.3).

afternoon. In the polluted situation, SOA mass production rate is higher after encountering Manaus at 8am. The maximum concentration is 1.5 µg $m^{-3}$, a 20% increase compared to the clean simulation. Even if the model is able to qualitatively reproduce the observed urban SOA enhancement, in the polluted situation the model still underestimates SOA mass by 30 to 50%.

### 4.2.2 Organosulfates

Figure 8 depicts modeled particle phase organosulfates, with mass concentrations ranging from 105 ng $m^{-3}$ in the morning to 205 ng $m^{-3}$ in the evening in the clean case scenario. The polluted situation increases late afternoon concentrations to 220 ng $m^{-3}$. These values are in the higher range of the reported measured range of 104±73 ng $m^{-3}$ in Glasius et al. (2018). This is consistent with Glasius et al. (2018) who reported that the main source of the measured organosulfates is IEPOX heterogeneous uptake, which is the only pathway represented in this model. Furthermore, this shows that the combination of the MCM 3.3.1 isoprene oxidation mechanism to produce IEPOX and the reactive uptake parameterization from Marais et al. (2016) is able to predict realistic levels of organosulfates, assuming that aerosol properties are also realistic (hygroscopicity, inorganic sulfates and pH).

https://doi.org/10.5194/acp-2019-1024
Preprint. Discussion started: 21 November 2019
© Author(s) 2019. CC BY 4.0 License.



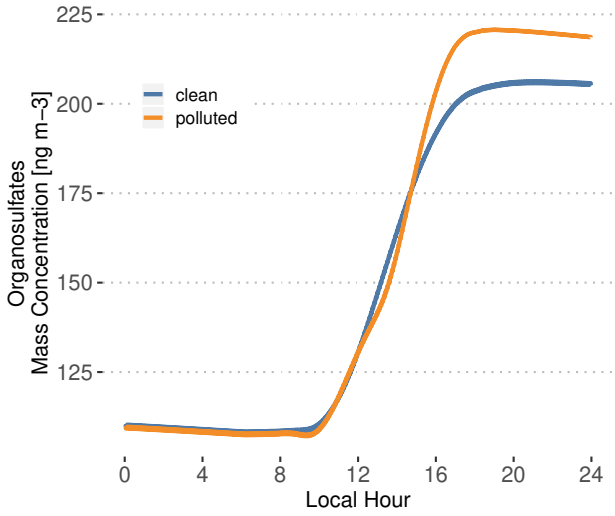


**Figure 8.** Modeled time evolution of particle phase organosulfates mass concentration. Cases are identified as clean (blue) and polluted (orange).

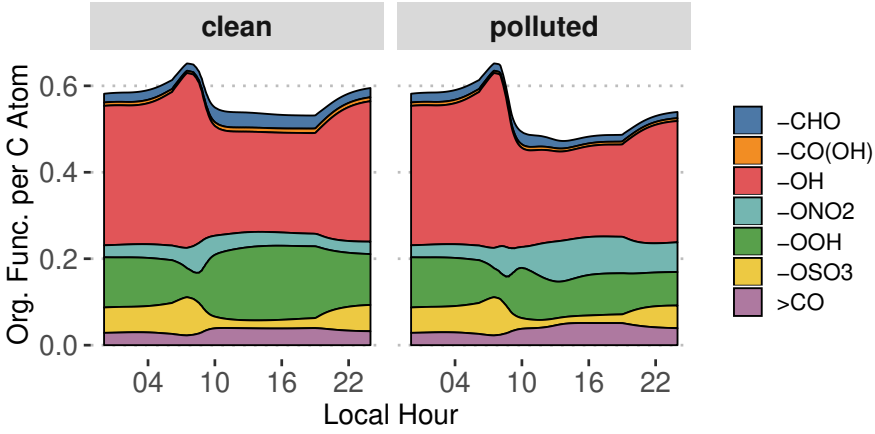


**Figure 9.** GECKO-A modeled time evolution of particle phase organic functionalization for the clean (left panel) and the polluted (right panel) cases. The y-axis is read as the number of a given organic function per carbon atom, i.e. in the clean case there is in total approximately one organic function for every two carbon atom.

### 4.2.3 Modeled Organic Functional Groups

280 Figure 9 depicts the distribution of organic functional groups in the particle phase. In the clean case scenario, total functionalization, defined as the number of functional groups per carbon atom, is constant around approximately 0.5. As expected for low-$NO_x$ situations, approximately 40% of these functional groups are hydroxy moieties and 20% of the organic functional

https://doi.org/10.5194/acp-2019-1024
Preprint. Discussion started: 21 November 2019
© Author(s) 2019. CC BY 4.0 License.



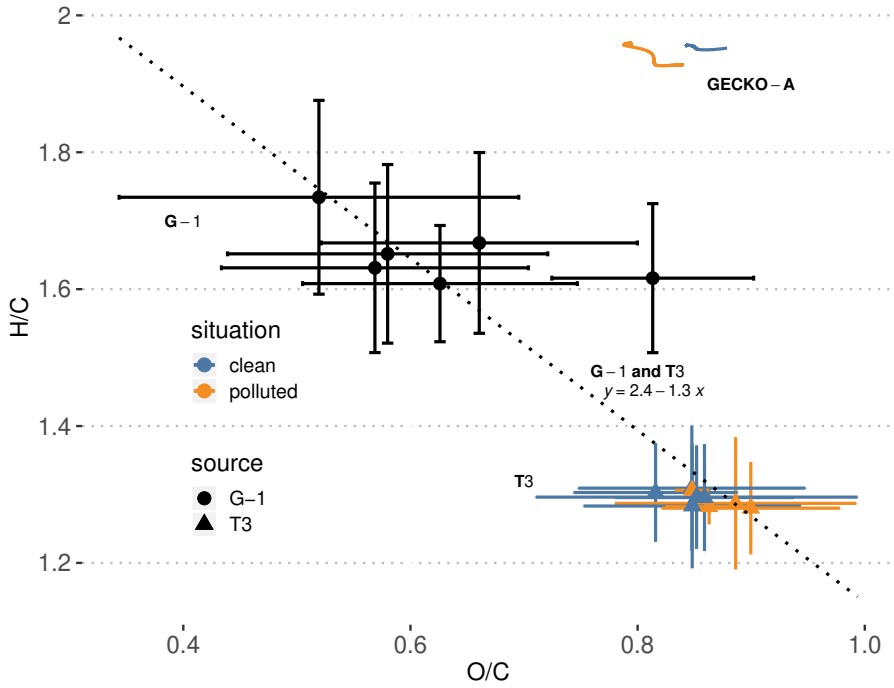


**Figure 10.** T3 site (colored triangles), airborne (black dots) and modeled (lines, afternoon of second day) van Krevelen diagrams of H/C (y-axis) vs O/C (x-axis) average ratios in SOA. The vertical and horizontal range of the experimental data denotes the standard deviation of measured concentrations. Cases are identified as clean (blue) and polluted (orange). Airborne data were filtered to only include measurements taken within 20 km of the T3 site. The dotted line and the associated equation depict the linear regression obtained with all experimental points (T3 and G-1).

groups are hydroperoxides. The remaining functional groups are dominated by carbonyls and nitrates to a lower extent. Manaus pollution has the direct effect of reducing total functionalization by 10% because of the contribution of long-chain primary hydrocarbons to SOA formation in the plume. Oxidation of organics in the higher $NO_x$ environment also leads to an increase of nitrate moieties contribution at the expense of hydroxy and hydroperoxide moieties.

#### 4.2.4 Modeled vs Measured Atomic Ratios

Figure 10 depicts simulated, ground measurements and airborne measurements of O/C and H/C atomic ratios in aerosol particles on a van Krevelen diagram. At the T3 site, experimental O/C ratios range from 0.7 to 1 in both clean and polluted conditions while H/C ratios range from 1.2 to 1.4. Additionally airborne measurements above the T3 site report O/C ratios ranging from 0.35 to 0.9 and H/C ratios ranging from 1.5 to 1.9. Compiling multiple field campaigns AMS measurements, Chen et al. (2015b) reported van Krevelen diagrams slopes (H/C vs O/C) ranging from -1 to -0.7. A linear regression over the data points from both airborne and ground measurements (dotted line on Fig. 10) gives a slope of -1.3, close to values reported

https://doi.org/10.5194/acp-2019-1024
Preprint. Discussion started: 21 November 2019
© Author(s) 2019. CC BY 4.0 License.



in Chen et al. (2015b). This means that T3 air masses are sampled at a later stage of oxidation than the airborne samples, possibly because they were exposed to higher levels of oxidants than the higher altitude air masses.

The modeled average particle phase O/C ratios range from 0.78 to 0.88, within the ratios measured at the T3 site. Modeled H/C ratios are however overestimated compared to T3 site measurements, ranging from 1.93 to 1.96. Claflin and Ziemann (2018) reported experimental evidence that the reaction of $\beta$-pinene with $NO_3$ produces oligomers derived from $\beta$-pinene $C_{10}$ oxidation products. For instance one of the proposed mechanisms for dimerization of a $C_{10}H_{17}O_5$ (H/C = 1.7) produces a $C_{20}H_{30}O_9$ (H/C = 1.5). In the GECKO-A modeled aerosol phase, after organosulfate and nitrates derived from isoprene, $C_{10}$ compounds dominate OA composition. As examples, a $C_{10}H_{18}O_7$ (H/C = 1.8; O/C = 0.7) and a $C_{10}H_{20}O_6$ (H/C = 2; O/C = 0.6) derived from limonene are the third and fourth most important organic species in the aerosol phase on a molecule basis. Following the dimerization pathways suggested by Claflin and Ziemann (2018), these compounds could potentially form $C_{20}H_{32}O_{13}$ (H/C = 1.6; O/C = 0.65) and $C_{20}H_{36}O_{11}$ (H/C = 1.8; O/C = 0.55) dimers respectively. Dimerization, or similar oligomerization processes, would then possibly move the modeled van Krevelen diagram towards lower H/C ratios, closer to AMS measurements.

Oppositely, GECKO-A could be missing processes that would fragment these two $C_{10}$ compounds. Fragmenting $C_{10}H_{18}O_7$ into a $C_4H_6O_4$ (H/C = 1.5; O/C = 1) and a $C_6H_{10}O_5$ (H/C = 1.7; O/C = 0.8) species would bring the average H/C ratio down from 1.8 to 1.6. This possibility of missing fragmentation processing means that either the modeled gas phase chemistry doesn't compete enough with condensation to fragment these species, or these $C_{10}$ species should be fragmented by heterogeneous or condensed phase processes in the particles themselves, which are not accounted for by the model. It should be noted that because the fragmented compounds are lighter, they would exhibit higher volatility. However this does not necessarily mean that the SOA mass would decrease because these shorter species are still oxygenated, maybe enough to contribute to SOA mass through solubility controlled processes in the same fashion as what is known about isoprene oxidation products.

### 4.3 Comparison with VBS approach

Shrivastava et al. (2019) modeled this same field campaign with WRF-Chem, a chemistry transport regional model (Grell et al., 2005). Using a Volatility Basis Set approach (VBS) to account for condensation of low volatility species, and considering ISOPSOA separately with an approach similar to this work, they modeled airborne SOA mass to within 15% of airborne measurements. The VBS parameterization described in Shrivastava et al. (2019) represents the formation of SOA as four surrogate species differing by their volatility ($C^\star$ = 0.1, 1, 10 and 100 µg $m^{-3}$). For biogenic SOA, isoprene and monoterpenes produce these four surrogates from the oxidation by OH, ozone and $NO_3$, with yields depending on $NO_x$. Moreover multigenerational aging is accounted for the surrogate species assigning fragmentation (*i.e.* increasing volatility) and functionalization (*i.e.* decreasing volatility). The yields used in this VBS approach were fitted over a variety of low OA loading atmospheric chamber studies of biogenics oxidation under high and low $NO_x$ concentrations (Shrivastava et al., 2019). More details about this VBS approach can be found in Shrivastava et al. (2013, 2015, 2019).

In order to compare the GECKO-A model results with the VBS approach used in Shrivastava et al. (2019), additional simulations were run where the explicit condensation of low volatility biogenic species was replaced by formation of the four

https://doi.org/10.5194/acp-2019-1024
Preprint. Discussion started: 21 November 2019
© Author(s) 2019. CC BY 4.0 License.



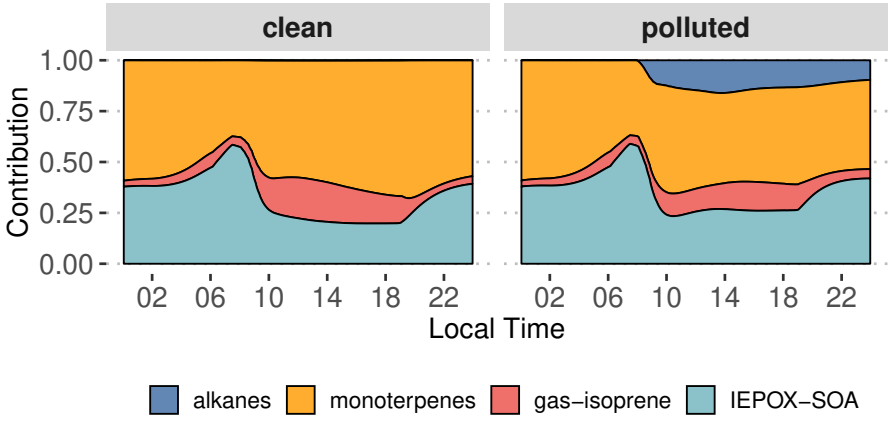


**Figure 11.** Contribution of primary hydrocarbons categories to GECKO-A modeled SOA mass for the clean (left panel) and polluted case (right panel).

surrogate species used in Shrivastava et al. (2019). Fig. 7 shows the time evolution of predicted SOA mass with GECKO-A, after replacing the original condensation of low volatility biogenic species by the VBS approach used in Shrivastava et al. (2019) (dashed lines). In this test, the VBS modeled SOA mass is well within the range of measured values in the polluted case scenario. The VBS version of the box-model is however underestimating SOA mass concentrations in the clean situation, with only 0.5 µg $m^{-3}$ during daytime compared to the measured 0.6 to 2.5 µg $m^{-3}$ range. Like in Shrivastava et al. (2019), exposure of the background air mass to the urban increased oxidative capacity increases VBS predicted SOA mass by almost 400%, which explains how the VBS can reach the higher polluted case SOA mass. Figure 7 also depicts the predicted SOA mass if SOA aging is not included in the VBS model (dotted lines). Shrivastava et al. (2019) reported that SOA aging does not have a strong effect in their simulations, which is not the case when applied in the box-model. In our simulation without aging processes, the polluted case SOA mass concentration drops below 1 µg $m^{-3}$. However in the clean case scenario, the SOA mass concentration only decreases by approximately 10% when SOA aging is removed. This means that SOA aging becomes more important in the ground case scenario when the air mass is exposed to high OH concentrations that were not seen by the model run by Shrivastava et al. (2019): their maximum OH concentrations reach $2\times10^{6}$ molec $cm^{-3}$ while our maximum OH concentration reach $1.6\times10^{7}$ molec $cm^{-3}$.

Figure 11 and Table 2 attribute sources of SOA according to the GECKO-A explicit simulation and the VBS approach. In the clean case scenario, GECKO-A attributes most of SOA mass to monoterpene oxidation products (60% at 2pm). The remainder is attributed to isoprene SOA, with condensation of low volatility compounds contributing in the same proportion as reactive uptake (19% and 21% respectively). In Shrivastava et al. (2019), monoterpene oxidation products account for 45% of SOA sources in the airborne plume. With their VBS applied to the ground situation, 31% of SOA is attributed to monoterpenes at 2pm, half of the proportion predicted by the GECKO-A explicit approach. Like in the 3D model calculation, the VBS in the

https://doi.org/10.5194/acp-2019-1024
Preprint. Discussion started: 21 November 2019
© Author(s) 2019. CC BY 4.0 License.



**Table 2.** Contribution of primary hydrocarbons categories to modeled SOA mass at 2pm. Percentages in parentheses indicate the relative contribution to total SOA mass.

| | GECKO-A | | VBS - aging | | VBS - no aging | | Measured[(a)] | |
|---|---|---|---|---|---|---|---|---|
| SOA mass [μg m$^{-3}$] | clean | polluted | clean | polluted | clean | polluted | | |
| Monoterpenes | 0.70 (60%) | 0.60 (44%) | 0.15 (31%) | 0.73 (32%) | 0.12 (28%) | 0.17 (18%) | – | – |
| Isoprene (gas) | 0.23 (19%) | 0.17 (13%) | 0.09 (19%) | 1.00 (43%) | 0.07 (16%) | 0.17 (18%) | – | – |
| IEPOX-SOA | 0.24 (21%) | 0.36 (27%) | 0.24 (50%) | 0.36 (16%) | 0.24 (56%) | 0.36 (40%) | – | – |
| biogenics | 1.17 (100%) | 1.13 (84%) | 0.48 (100%) | 2.09 (91%) | 0.43 (100%) | 0.70(76%) | – | – |
| anthropogenics | 0 (0%) | 0.22 (16%) | 0 (0%) | 0.22 (9%) | 0 (0%) | 0.22 (24%) | – | – |
| total | 1.17 | 1.35 | 0.48 | 2.31 | 0.43 | 0.92 | 1.4±0.8 | 2.1±0.2 |

[(a)]de Sá et al. (2018)

box model attributes the remainder of background SOA mass mostly to reactive uptake of isoprene oxidation products (50% of total SOA).

In the polluted case, the explicit model predicts an increase of 15% in total SOA at 2pm while measurements exhibit an increase of 33% on average. The urban effect is stronger in the VBS case than the explicit approach with a 380% increase in mass. In the comparison with airborne measurements, the Shrivastava et al. (2019) model predicts that the city oxidants cause the same large increase in biogenic SOA formation (up to 400%), and that this increase is due to enhanced monoterpene oxidation. With GECKO-A at the ground site, most of the SOA increase is due to the contribution of anthropogenics. In fact biogenic SOA remains constant (3% decrease) with respect to the clean case. In particular biogenic SOA produced by condensation of low volatility oxidation products of monoterpenes and isoprene decreases by 17%. This loss is compensated for by an increase in the production of SOA via reactive uptake of isoprene oxidation products (50% increase) because the plume favors these processes with higher sulfate load and lower pH (see Table 1). In the VBS test case, the SOA mass formed from condensation of low volatility oxidation products of isoprene and monoterpenes is enhanced in the polluted case respectively by a factor of 11 and 4.9. This enhancement is notably inhibited when the aging parameterization is removed from the VBS approach with a mass increase due to condensation of low volatility products of isoprene and monoterpenes of respectively 42% and 143%. This highlights the importance of modeling aging of low volatility oxidation products to explain the enhanced production of SOA in the urban plume.

### 4.4 Potential for Reduction of the Explicit GECKO-A mechanism

It is obvious that the chemical mechanisms generated with GECKO-A are too large to be implemented in 3D models. The GECKO-A mechanisms need to be reduced to sizes manageable by 3D models, typically a few hundred species and reactions. The VBS parameterization used for comparison in this work is fit for low OA loadings, biogenic dominated situations but it is unclear that it should be applied to other situations.

https://doi.org/10.5194/acp-2019-1024
Preprint. Discussion started: 21 November 2019
© Author(s) 2019. CC BY 4.0 License.



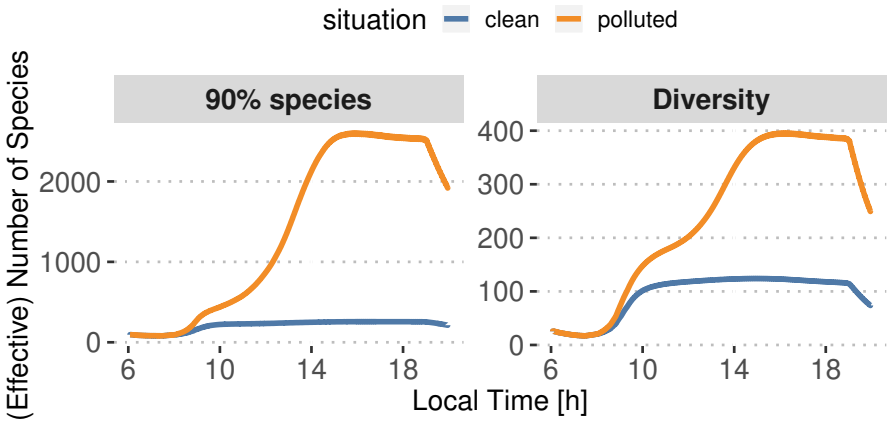


**Figure 12.** Minimum number of species needed to model 90% of SOA mass (left panel) with GECKO-A. Statistical diversity in the GECKO-A modeled particle phase, see Eq. 3 (right panel).

In this section, we are *not* proposing a much needed new approach to reducing explicit mechanisms with the goal of predicting SOA mass concentrations, but we explore here the potential for reduction of the chemical mechanism that was generated for this study. In other words, what is the theoretical lower limit to the number of species that should be used in a reduced scheme to still be able to model the same SOA mass concentration time profile as the explicit model?

To answer this, two metrics are presented in Fig. 12. The first one is the minimum number of species needed in the explicit model to represent at least 90% of the total SOA mass at each timestep. The second one is the particle diversity $D$ in the explicitly modeled SOA, as defined for instance in Riemer and West (2013):

$$D = \exp S \tag{3}$$

where $S$ is the first order generalized entropy (also known as Shannon entropy):

$$S = \sum_{i=1}^{N} -p_i \ln p_i \tag{4}$$

where $p_i$ is the mass fraction of species $i$ in the organic particle phase and $N$ is the total number of species in the organic particle phase. As stated in Riemer and West (2013), the diversity is a measure of the effective number of species with the same concentration in the organic fraction of the aerosol phase. If $D = 1$, the organic fraction is pure as it is composed of a single species. Therefore, a value $D \ll N$ means that of all the species contributing to modeled organic aerosol, only a few significantly contribute to its composition. Oppositely, $D = N$ is the maximum value reachable by $D$ and is obtained when the organic fraction is composed of $N$ equally distributed species. In the case where $D$ is close to $N$, only a few species are negligible. For more details and better explanations, we refer the reader to Riemer and West (2013, esp. Fig. 1). We make the hypothesis here that $D$ can be interpreted as an effective number of species derived from the informational entropy of the modeled particle phase.

https://doi.org/10.5194/acp-2019-1024
Preprint. Discussion started: 21 November 2019
© Author(s) 2019. CC BY 4.0 License.



In the clean situation both metrics behave similarly, with a morning increase of the number of species until 10 am, after which the number remains relatively constant until sunset. During daytime, on average 310 species are needed to represent 90% of the SOA mass. The calculated diversity is around 170 effective species. For the polluted situation, the number of species needed to represent 90% of the SOA mass during daytime increases by about a factor of 7, reaching about 2300. The calculated diversity only increases up to approximately 410 effective species. These increases in the species numbers for the polluted case are logical as the variety of precursors, and hence secondary species that could potentially contribute to SOA, is increased by urban emissions.

The number of species needed to represent most of the modeled SOA mass in all cases seems too high to be used in 3D models applications. Furthermore there is no guarantee that the most important species at a given timestep would be the same most important species at the following timestep. This suggests that reductions should not come from simply selecting species identified as important to represent the variety of species that could arise in the interaction of biogenic air and an urban plume.

The statistical diversity calculation seems like a better approach to estimate the minimum number of species needed to model SOA mass. As this number is directly derived from informational entropy, we suggest that the diversity represents the number of species that would be needed to reproduce the same informational content regarding the composition of SOA in the explicit model. Even if the effective species numbers fall in the higher range of what would be acceptable in a 3D model chemical mechanism, the practical construction of the mechanism remains to be explored. For instance, nothing here says that the effective species would be individual species already present in the original explicit mechanism. It is possible, and making this problem more complex, that each of these effective species is a (non) linear combination of explicit individual species.

## 5 Conclusions

An explicit chemical mechanism generated with GECKO-A was used in a box model to simulate a situation similar to the situation studied in Manaus during the GoAmazon 2014/5 field campaign. After scaling down the emissions generated from the MEGAN biogenic emissions model and estimating urban emissions in Manaus, the model was able to reproduce realistic primary organic compounds mixing ratios as well as $NO_x$, ozone and OH concentrations.

The model is able to reproduce background SOA mass concentrations but is not able to reproduce the observed enhancement in the polluted plume. When running a Volatility Basis Set approach that was previously applied to the Manaus case (Shrivastava et al., 2019), modeled SOA mass matches measurements which suggests that the incorrect explicit model prediction is not caused by incorrect primary organic compound emissions or oxidant levels. Modeled particle phase organosulfates are within the range of previous measurements (Glasius et al., 2018) which suggests that isoprene oxidation and SOA formation in the model are reasonably well simulated. In both polluted and clean situations, biogenics are identified as the main contributors to SOA by both GECKO-A and the VBS parameterization. In both approaches, the majority of SOA production is attributed to monoterpenes oxidation and condensation of lower volatility products. Yee et al. (2018) measured and described sesquiterpenes during GoAmazon 2014/5 for the same situations and suggested that these species may be important for modeling studies. However the modeling study of Shrivastava et al. (2019) estimated that the contribution of sesquiterpenes to

https://doi.org/10.5194/acp-2019-1024
Preprint. Discussion started: 21 November 2019
© Author(s) 2019. CC BY 4.0 License.



SOA production is less than 10%. It is more likely that physico-chemical processes involved in monoterpene SOA formation are either unknown or missing in the explicit model. Comparison of modeled and measured elemental ratios (H/C and O/C) indicates that fragmentation of monoterpenes oxidation products and their condensation or reactive uptake to the condensed phase may play an important role in understanding the sources of biogenic SOA mass. This reactive uptake may in turn involve oligomerization and fragmentation processes. Because the VBS parameterization is based on multiple chamber experiments, it could implicitly be accounting for these missing processes. Of the high diversity of monoterpenes identified in Amazonia (Jardine et al., 2015), only a handful of monoterpenes have been studied to the extent that we can be as confident in model predictions of SOA formation from monoterpenes as from isoprene. Detailed mechanistic studies of monoterpene oxidation are therefore needed for further incorporation in explicit models to better understand the nature and the magnitude of the contribution of monoterpenes to SOA formation, as well as their response to the interaction with urban pollution (*e.g.* Claflin and Ziemann, 2018).

Even if a parameterization was implemented in GECKO-A to properly address the formation of isoprene SOA via aqueous phase processes (Marais et al., 2016), to explicitly treat these in a more general way, future GECKO-A developments for mechanism generation will need to include the following: (i) aerosol thermodynamics, for instance via coupling with a model like MOSAIC (Zaveri et al., 2008) or ISORROPIA (Nenes et al., 1998), (ii) aqueous phase processes including explicit dissolution (*e.g.* Mouchel-Vallon et al., 2013), oxidation (*e.g.* Mouchel-Vallon et al., 2017), accretion reactions (*e.g.* Renard et al., 2015), and interaction with dissolved inorganic ions, (iii) explicit treatment of the fate of newly formed species like dimers or organo-sulfates.

One could be tempted to think that since the VBS parameterization is behaving particularly well in this GoAmazon 2014/5 case, it could be the answer to predict SOA mass in larger scale 3D models. However this approach is limited by the fact that it was fitted for low biogenic OA loading situations and was run in a limited domain regional model (Shrivastava et al., 2019). One possible way of building reduced mechanisms is to reduce existing detailed chemical mechanisms to sizes manageable by 3D models (e.g. Szopa et al., 2005; Kaduwela et al., 2015). Using an information theory based approach, we provide here a lower limit to the size of these reduced mechanisms, assuming the goal is to produce the same informational content as the explicit mechanism. This lower limit of a few hundred species is four orders of magnitudes lower than the actual number of species that are actually accounted for in the explicit mechanism ($4\times10^6$) and shows the potential for progress in future mechanism reduction endeavors. Even if a direct application of this statistical approach to create a reduced mechanism would likely require some atmospheric chemistry breakthrough, it could at least currently be used as a statistical indicator for comparing reduced mechanisms with reference explicit mechanisms.

*Competing interests.* The authors declare no competing interests.

https://doi.org/10.5194/acp-2019-1024
Preprint. Discussion started: 21 November 2019
© Author(s) 2019. CC BY 4.0 License.

Atmospheric Chemistry and Physics Discussions

*Acknowledgements.* The National Center for Atmospheric Research is sponsored by the National Science Foundation. We gratefully acknowledge support from U.S. Department of Energy (DOE) ASR grant DE-SC0016331. JLJ and BBP were supported by NSF AGS-1822664 and EPA 83587701-0. This manuscript has not been reviewed by EPA, and thus no endorsement should be inferred. Dr. Shrivastava was also supported by the U.S. DOE, Office of Science, Office of Biological and Environmental Research through the Early Career Research Program. Data were obtained from the Atmospheric Radiation Measurement (ARM) User Facility, a U.S. DOE Office of Science user facility managed by the Office of Biological and Environmental Research. The research was conducted under scientific license 001030/2012-4 of the Brazilian National Council for Scientific and Technological Development (CNPq). We are grateful to Louisa K. Emmons for providing the MEGAN emissions data; and Suzane S. de Sà for providing the clustering analysis results. We are thanking Siyuan Wang for helpful comments.

https://doi.org/10.5194/acp-2019-1024
Preprint. Discussion started: 21 November 2019
© Author(s) 2019. CC BY 4.0 License.



## References

Abou Rafee, S. A., Martins, L. D., Kawashima, A. B., Almeida, D. S., Morais, M. V. B., Souza, R. V. A., Oliveira, M. B. L., Souza, R. A. F., Medeiros, A. S. S., Urbina, V., Freitas, E. D., Martin, S. T., and Martins, J. A.: Contributions of mobile, stationary and biogenic sources to air pollution in the Amazon rainforest: a numerical study with the WRF-Chem model, Atmospheric Chemistry and Physics, 17, 7977–7995, https://doi.org/10.5194/acp-17-7977-2017, 2017.

Altieri, K. E., Carlton, A. G., Lim, H.-J., Turpin, B. J., and Seitzinger, S. P.: Evidence for oligomer formation in clouds: reactions of isoprene oxidation products., Environmental science & technology, 40, 4956–60, 2006.

Alves, E. G., Jardine, K., Tota, J., Jardine, A., Yãnez-Serrano, A. M., Karl, T., Tavares, J., Nelson, B., Gu, D., Stavrakou, T., Martin, S., Artaxo, P., Manzi, A., and Guenther, A.: Seasonality of isoprenoid emissions from a primary rainforest in central Amazonia, Atmospheric Chemistry and Physics, 16, 3903–3925, https://doi.org/10.5194/acp-16-3903-2016, 2016.

Andrade, M. D. F., Ynoue, R. Y., Freitas, E. D., Todesco, E., Vara Vela, A., Ibarra, S., Martins, L. D., Martins, J. A., and Carvalho, V. S. B.: Air quality forecasting system for Southeastern Brazil, Frontiers in Environmental Science, 3, 6975, https://doi.org/10.3389/fenvs.2015.00009, 2015.

Aumont, B., Szopa, S., and Madronich, S.: Modelling the evolution of organic carbon during its gas-phase tropospheric oxidation: development of an explicit model based on a self generating approach, Atmospheric Chemistry and Physics, 5, 2497–2517, https://doi.org/10.5194/acp-5-2497-2005, 2005.

Aumont, B., Valorso, R., Mouchel-Vallon, C., Camredon, M., Lee-Taylor, J., and Madronich, S.: Modeling SOA formation from the oxidation of intermediate volatility n-alkanes, Atmospheric Chemistry and Physics, 12, 7577–7589, https://doi.org/10.5194/acp-12-7577-2012, 2012.

Aumont, B., Camredon, M., Mouchel-Vallon, C., La, S., Ouzebidour, F., Valorso, R., Lee-Taylor, J., and Madronich, S.: Modeling the influence of alkane molecular structure on secondary organic aerosol formation, Faraday Discussions, 165, 105, https://doi.org/10.1039/c3fd00029j, 2013.

Batista, C. E., Ye, J., Ribeiro, I. O., Guimarães, P. C., Medeiros, A. S. S., Barbosa, R. G., Oliveira, R. L., Duvoisin, S., Jardine, K. J., Gu, D., Guenther, A. B., McKinney, K. A., Martins, L. D., Souza, R. A. F., and Martin, S. T.: Intermediate-scale horizontal isoprene concentrations in the near-canopy forest atmosphere and implications for emission heterogeneity, Proceedings of the National Academy of Sciences, p. 201904154, https://doi.org/10.1073/pnas.1904154116, 2019.

Bezdek, J. C.: Pattern recognition with fuzzy objective function algorithms, Plenum, New York, 1981.

Bezdek, J. C., Ehrlich, R., and Full, W.: FCM: The fuzzy c-means clustering algorithm, Computers & Geosciences, 10, 191–203, https://doi.org/10.1016/0098-3004(84)90020-7, 1984.

Blando, J. D. and Turpin, B. J.: Secondary organic aerosol formation in cloud and fog droplets: a literature evaluation of plausibility, Atmospheric Environment, 34, 1623–1632, 2000.

Browell, E. V., Gregory, G. L., Harriss, R. C., and Kirchhoff, V. W. J. H.: Ozone and aerosol distributions over the Amazon Basin during the wet season, Journal of Geophysical Research, 95, 16 887, https://doi.org/10.1029/JD095iD10p16887, 1990.

Budisulistiorini, S. H., Baumann, K., Edgerton, E. S., Bairai, S. T., Mueller, S., Shaw, S. L., Knipping, E. M., Gold, A., and Surratt, J. D.: Seasonal characterization of submicron aerosol chemical composition and organic aerosol sources in the southeastern United States: Atlanta, Georgia, and Look Rock, Tennessee, Atmospheric Chemistry and Physics, 16, 5171–5189, https://doi.org/10.5194/acp-16-5171-2016, 2016.

Camredon, M. and Aumont, B.: Assessment of vapor pressure estimation methods for secondary organic aerosol modeling, Atmospheric Environment, 40, 2105–2116, https://doi.org/10.1016/j.atmosenv.2005.11.051, 2006.

Camredon, M., Aumont, B., Lee-Taylor, J., and Madronich, S.: The SOA/VOC/NOx system: an explicit model of secondary organic aerosol formation, Atmospheric Chemistry and Physics, 7, 5599–5610, https://doi.org/10.5194/acp-7-5599-2007, 2007.

Carlton, A. G., Wiedinmyer, C., and Kroll, J. H.: A review of Secondary Organic Aerosol (SOA) formation from isoprene, Atmospheric Chemistry and Physics, 9, 4987–5005, https://doi.org/10.5194/acp-9-4987-2009, 2009.

Chen, Q., Farmer, D. K., Rizzo, L. V., Pauliquevis, T., Kuwata, M., Karl, T. G., Guenther, A., Allan, J. D., Coe, H., Andreae, M. O., Pöschl, U., Jimenez, J. L., Artaxo, P., and Martin, S. T.: Submicron particle mass concentrations and sources in the Amazonian wet season (AMAZE-08), Atmospheric Chemistry and Physics, 15, 3687–3701, https://doi.org/10.5194/acp-15-3687-2015, https://www.atmos-chem-phys.net/15/3687/2015/, 2015a.

Chen, Q., Heald, C. L., Jimenez, J. L., Canagaratna, M. R., Zhang, Q., He, L.-y., Huang, X.-f., Campuzano-jost, P., Palm, B. B., Poulain, L., Kuwata, M., Martin, S. T., Abbatt, J. P. D., Lee, A. K. Y., and Liggio, J.: Elemental composition of organic aerosol: The gap between ambient and laboratory measurements, Geophys. Res. Lett., 42, 4182–4189, https://doi.org/10.1002/2015GL063693.Received, 2015b.

Claeys, M.: Formation of Secondary Organic Aerosols Through Photooxidation of Isoprene, Science, 303, 1173–1176, https://doi.org/10.1126/science.1092805, 2004.

Claflin, M. S. and Ziemann, P. J.: Identification and Quantitation of Aerosol Products of the Reaction of $\beta$-Pinene with NO 3 Radicals and Implications for Gas- and Particle-Phase Reaction Mechanisms, The Journal of Physical Chemistry A, p. acs.jpca.8b00692, https://doi.org/10.1021/acs.jpca.8b00692, 2018.

Computational and Information Systems Laboratory: Cheyenne: HPE/SGI ICE XA System (NCAR Community Computing), https://doi.org/10.5065/D6RX99HX, 2017.

Daumit, K. E., Carrasquillo, A. J., Sugrue, R. A., and Kroll, J. H.: Effects of Condensed-Phase Oxidants on Secondary Organic Aerosol Formation, The Journal of Physical Chemistry A, 120, 1386–1394, https://doi.org/10.1021/acs.jpca.5b06160, 2016.

de Sá, S. S., Palm, B. B., Campuzano-jost, P., Day, D. A., Newburn, M. K., Hu, W., Isaacman-VanWertz, G., Yee, L. D., Thalman, R., Brito, J., Carbone, S., Artaxo, P., Goldstein, A. H., Manzi, A. O., Souza, R. A. F., Mei, F., Shilling, J. E., Springston, S. R., Wang, J., Surratt, J. D., Alexander, M. L., Jimenez, J. L., and Martin, S. T.: Influence of urban pollution on the production of organic particulate matter from isoprene epoxydiols in central Amazonia, Atmospheric Chemistry and Physics, 17, 6611–6629, https://doi.org/10.5194/acp-17-6611-2017, 2017.

de Sá, S. S., Palm, B. B., Campuzano-Jost, P., Day, D. A., Hu, W., Isaacman-VanWertz, G., Yee, L. D., Brito, J., Carbone, S., Ribeiro, I. O., Cirino, G. G., Liu, Y., Thalman, R., Sedlacek, A., Funk, A., Schumacher, C., Shilling, J. E., Schneider, J., Artaxo, P., Goldstein, A. H., Souza, R. A. F., Wang, J., McKinney, K. A., Barbosa, H., Alexander, M. L., Jimenez, J. L., and Martin, S. T.: Urban influence on the concentration and composition of submicron particulate matter in central Amazonia, Atmospheric Chemistry and Physics, 18, 12 185–12 206, https://doi.org/10.5194/acp-18-12185-2018, 2018.

de Sá, S. S., Rizzo, L. V., Palm, B. B., Campuzano-Jost, P., Day, D. A., Yee, L. D., Wernis, R., Isaacman-VanWertz, G., Brito, J., Carbone, S., Liu, Y. J., Sedlacek, A., Springston, S., Goldstein, A. H., Barbosa, H. M. J., Alexander, M. L., Artaxo, P., Jimenez, J. L., and Martin, S. T.: Contributions of biomass-burning, urban, and biogenic emissions to the concentrations and light-absorbing properties of particulate matter in central Amazonia during the dry season, Atmospheric Chemistry and Physics, 19, 7973–8001, https://doi.org/10.5194/acp-19-7973-2019, 2019.

DeCarlo, P. F., Kimmel, J. R., Trimborn, A., Northway, M. J., Jayne, J. T., Aiken, A. C., Gonin, M., Fuhrer, K., Horvath, T., Docherty, K. S., Worsnop, D. R., and Jimenez, J. L.: Field-Deployable, High-Resolution, Time-of-Flight Aerosol Mass Spectrometer, Analytical Chemistry, 78, 8281–8289, https://doi.org/10.1021/ac061249n, 2006.

Donahue, N. M., Robinson, A. L., Stanier, C. O., and Pandis, S. N.: Coupled Partitioning, Dilution, and Chemical Aging of Semivolatile Organics, Environmental Science & Technology, 40, 2635–2643, https://doi.org/10.1021/es052297c, 2006.

Ervens, B., Turpin, B. J., and Weber, R. J.: Secondary organic aerosol formation in cloud droplets and aqueous particles (aqSOA): a review of laboratory, field and model studies, Atmospheric Chemistry and Physics, 11, 11 069–11 102, 2011.

Gentner, D. R., Isaacman, G., Worton, D. R., Chan, A. W. H., Dallmann, T. R., Davis, L., Liu, S., Day, D. A., Russell, L. M., Wilson, K. R., Weber, R., Guha, A., Harley, R. A., and Goldstein, A. H.: Elucidating secondary organic aerosol from diesel and gasoline vehicles through detailed characterization of organic carbon emissions, Proceedings of the National Academy of Sciences, 109, 18 318–18 323, https://doi.org/10.1073/pnas.1212272109, 2012.

Gentner, D. R., Jathar, S. H., Gordon, T. D., Bahreini, R., Day, D. A., El Haddad, I., Hayes, P. L., Pieber, S. M., Platt, S. M., De Gouw, J., Goldstein, A. H., Harley, R. A., Jimenez, J. L., Prévôt, A. S., and Robinson, A. L.: Review of Urban Secondary Organic Aerosol Formation from Gasoline and Diesel Motor Vehicle Emissions, Environmental Science and Technology, 51, 1074–1093, https://doi.org/10.1021/acs.est.6b04509, 2017.

Glasius, M., Bering, M. S., Yee, L. D., De Sá, S. S., Isaacman-VanWertz, G., Wernis, R. A., Barbosa, H. M., Alexander, M. L., Palm, B. B., Hu, W., Campuzano-Jost, P., Day, D. A., Jimenez, J. L., Shrivastava, M., Martin, S. T., and Goldstein, A. H.: Organosulfates in aerosols downwind of an urban region in central Amazon, Environmental Science: Processes and Impacts, 20, 1546–1558, https://doi.org/10.1039/c8em00413g, 2018.

Gregory, G. L., Browell, E. V., Warren, L. S., and Hudgins, C. H.: Amazon Basin ozone and aerosol: Wet season observations, Journal of Geophysical Research, 95, 16 903, https://doi.org/10.1029/JD095iD10p16903, 1990.

Grell, G. A., Peckham, S. E., Schmitz, R., McKeen, S. A., Frost, G., Skamarock, W. C., and Eder, B.: Fully coupled "online" chemistry within the WRF model, Atmospheric Environment, 39, 6957–6975, https://doi.org/10.1016/j.atmosenv.2005.04.027, 2005.

Guenther, A. B., Jiang, X., Heald, C. L., Sakulyanontvittaya, T., Duhl, T., Emmons, L. K., and Wang, X.: The model of emissions of gases and aerosols from nature version 2.1 (MEGAN2.1): An extended and updated framework for modeling biogenic emissions, Geoscientific Model Development, 5, 1471–1492, https://doi.org/10.5194/gmd-5-1471-2012, 2012.

Jardine, A. B., Jardine, K. J., Fuentes, J. D., Martin, S. T., Martins, G., Durgante, F., Carneiro, V., Higuchi, N., Manzi, A. O., and Chambers, J. Q.: Highly reactive light-dependent monoterpenes in the Amazon, Geophysical Research Letters, 42, 1576–1583, https://doi.org/10.1002/2014GL062573, 2015.

Jenkin, M. E., Saunders, S. M., and Pilling, M. J.: The tropospheric degradation of volatile organic compounds: A protocol for mechanism development, Atmospheric Environment, 31, 81–104, 1997.

Jenkin, M. E., Young, J. C., and Rickard, a. R.: The MCM v3.3.1 degradation scheme for isoprene, Atmospheric Chemistry and Physics, 15, 11 433–11 459, https://doi.org/10.5194/acp-15-11433-2015, 2015.

Jo, D. S., Hodzic, A., Emmons, L. K., Marais, E. A., Peng, Z., Nault, B. A., Hu, W., Campuzano-Jost, P., and Jimenez, J. L.: A simplified parameterization of isoprene-epoxydiol-derived secondary organic aerosol (IEPOX-SOA) for global chemistry and climate models: a case study with GEOS-Chem v11-02-rc, Geoscientific Model Development, 12, 2983–3000, https://doi.org/10.5194/gmd-12-2983-2019, 2019.

Jordan, A., Haidacher, S., Hanel, G., Hartungen, E., Herbig, J., Märk, L., Schottkowsky, R., Seehauser, H., Sulzer, P., and Märk, T.: An online ultra-high sensitivity Proton-transfer-reaction mass-spectrometer combined with switchable reagent ion capability (PTR+SRI-MS), International Journal of Mass Spectrometry, 286, 32–38, https://doi.org/10.1016/j.ijms.2009.06.006, 2009a.

Jordan, A., Haidacher, S., Hanel, G., Hartungen, E., Märk, L., Seehauser, H., Schottkowsky, R., Sulzer, P., and Märk, T.: A high resolution and high sensitivity proton-transfer-reaction time-of-flight mass spectrometer (PTR-TOF-MS), International Journal of Mass Spectrometry, 286, 122–128, https://doi.org/10.1016/j.ijms.2009.07.005, 2009b.

Kaduwela, A., Luecken, D., Carter, W., and Derwent, R.: New directions: Atmospheric chemical mechanisms for the future, Atmospheric Environment, 122, 609–610, https://doi.org/10.1016/j.atmosenv.2015.10.031, 2015.

Kirchhoff, V. W. J. H., da Silva, I. M. O., and Browell, E. V.: Ozone measurements in Amazonia: Dry season versus wet season, Journal of Geophysical Research, 95, 16 913, https://doi.org/10.1029/JD095iD10p16913, 1990.

Koss, A., Yuan, B., Warneke, C., Gilman, J. B., Lerner, B. M., Veres, P. R., Peischl, J., Eilerman, S., Wild, R., Brown, S. S., Thompson, C. R., Ryerson, T., Hanisco, T., Wolfe, G. M., St Clair, J. M., Thayer, M., Keutsch, F. N., Murphy, S., and De Gouw, J.: Observations of VOC emissions and photochemical products over US oil- and gas-producing regions using high-resolution H3O+CIMS (PTR-ToF-MS), Atmospheric Measurement Techniques, 10, 2941–2968, https://doi.org/10.5194/amt-10-2941-2017, 2017a.

Koss, A. R., Sekimoto, K., Gilman, J. B., Selimovic, V., Coggon, M. M., Zarzana, K. J., Yuan, B., Lerner, B. M., Brown, S. S., Jimenez, J. L., Krechmer, J., Roberts, J. M., Warneke, C., Yokelson, R. J., and de Gouw, J.: Non-methane organic gas emissions from biomass burning: identification, quantification, and emission factors from PTR-ToF during the FIREX 2016 laboratory experiment, Atmospheric Chemistry and Physics Discussions, pp. 1–44, https://doi.org/10.5194/acp-2017-924, 2017b.

La, Y. S., Camredon, M., Ziemann, P. J., Valorso, R., Matsunaga, A., Lannuque, V., Lee-Taylor, J., Hodzic, A., Madronich, S., and Aumont, B.: Impact of chamber wall loss of gaseous organic compounds on secondary organic aerosol formation: explicit modeling of SOA formation from alkane and alkene oxidation, Atmospheric Chemistry and Physics, 16, 1417–1431, https://doi.org/10.5194/acp-16-1417-2016, 2016.

Lee-Taylor, J., Madronich, S., Aumont, B., Baker, A., Camredon, M., Hodzic, A., Tyndall, G. S., Apel, E., and Zaveri, R. a.: Explicit modeling of organic chemistry and secondary organic aerosol partitioning for Mexico City and its outflow plume, Atmospheric Chemistry and Physics, 11, 13 219–13 241, https://doi.org/10.5194/acp-11-13219-2011, 2011.

Lee-Taylor, J., Hodzic, A., Madronich, S., Aumont, B., Camredon, M., and Valorso, R.: Multiday production of condensing organic aerosol mass in urban and forest outflow, Atmospheric Chemistry and Physics, 15, 595–615, https://doi.org/10.5194/acp-15-595-2015, 2015.

Lenschow, D. H., Gurarie, D., and Patton, E. G.: Modeling the diurnal cycle of conserved and reactive species in the convective boundary layer using SOMCRUS, Geoscientific Model Development, 9, 979–996, https://doi.org/10.5194/gmd-9-979-2016, 2016.

Liu, Y., Siekmann, F., Renard, P., El Zein, A., Salque, G., El Haddad, I., Temime-Roussel, B., Voisin, D., Thissen, R., and Monod, A.: Oligomer and SOA formation through aqueous phase photooxidation of methacrolein and methyl vinyl ketone, Atmospheric Environment, 49, 123–129, https://doi.org/10.1016/j.atmosenv.2011.12.012, 2012.

Liu, Y., Seco, R., Kim, S., Guenther, A. B., Goldstein, A. H., Keutsch, F. N., Springston, S. R., Watson, T. B., Artaxo, P., Souza, R. A., McKinney, K. A., and Martin, S. T.: Isoprene photo-oxidation products quantify the effect of pollution on hydroxyl radicals over Amazonia, Science Advances, 4, 1–9, https://doi.org/10.1126/sciadv.aar2547, 2018.

Marais, E. A., Jacob, D. J., Jimenez, J. L., Campuzano-Jost, P., Day, D. A., Hu, W., Krechmer, J., Zhu, L., Kim, P. S., Miller, C. C., Fisher, J. A., Travis, K., Yu, K., Hanisco, T. F., Wolfe, G. M., Arkinson, H. L., Pye, H. O. T., Froyd, K. D., Liao, J., and McNeill, V. F.: Aqueous-

phase mechanism for secondary organic aerosol formation from isoprene: application to the southeast United States and co-benefit of SO2 emission controls, Atmospheric Chemistry and Physics, 16, 1603–1618, https://doi.org/10.5194/acp-16-1603-2016, 2016.

Martin, S. T., Andreae, M. O., Artaxo, P., Baumgardner, D., Chen, Q., Goldstein, A. H., Guenther, A., Heald, C. L., Mayol-Bracero, O. L., McMurry, P. H., Pauliquevis, T., Pöschl, U., Prather, K. A., Roberts, G. C., Saleska, S. R., Silva Dias, M. A., Spracklen, D. V., Swietlicki, E., and Trebs, I.: Sources and properties of Amazonian aerosol particles, Reviews of Geophysics, 48, RG2002, https://doi.org/10.1029/2008RG000280, 2010.

Martin, S. T., Artaxo, P., Machado, L. A. T., Manzi, A. O., Souza, R. A. F., Schumacher, C., Wang, J., Andreae, M. O., Barbosa, H. M. J., Fan, J., Fisch, G., Goldstein, A. H., Guenther, A., Jimenez, J. L., Pöschl, U., Silva Dias, M. A., Smith, J. N., and Wendisch, M.: Introduction: Observations and Modeling of the Green Ocean Amazon (GoAmazon2014/5), Atmospheric Chemistry and Physics, 16, 4785–4797, https://doi.org/10.5194/acp-16-4785-2016, 2016.

Martins, L. D., Andrade, M. F., Freitas, E. D., Pretto, A., Gatti, L. V., Albuquerque, É. L., Tomaz, E., Guardani, M. L., Martins, M. H. R. B., and Junior, O. M. A.: Emission factors for gas-powered vehicles traveling through road tunnels in São Paulo, Brazil, Environmental Science and Technology, 40, 6722–6729, https://doi.org/10.1021/es052441u, 2006.

McNeill, V. F., Woo, J. L., Kim, D. D., Schwier, A. N., Wannell, N. J., Sumner, A. J., and Barakat, J. M.: Aqueous-Phase Secondary Organic Aerosol and Organosulfate Formation in Atmospheric Aerosols: A Modeling Study, Environmental Science & Technology, 46, 8075–8081, https://doi.org/10.1021/es3002986, 2012.

Mouchel-Vallon, C., Bräuer, P., Camredon, M., Valorso, R., Madronich, S., Herrmann, H., and Aumont, B.: Explicit modeling of volatile organic compounds partitioning in the atmospheric aqueous phase, Atmospheric Chemistry and Physics, 13, 1023–1037, https://doi.org/10.5194/acp-13-1023-2013, 2013.

Mouchel-Vallon, C., Deguillaume, L., Monod, A., Perroux, H., Rose, C., Ghigo, G., Long, Y., Leriche, M., Aumont, B., Patryl, L., Armand, P., and Chaumerliac, N.: CLEPS 1.0: A new protocol for cloud aqueous phase oxidation of VOC mechanisms, Geoscientific Model Development, 10, 1339–1362, https://doi.org/10.5194/gmd-10-1339-2017, 2017.

Nannoolal, Y., Rarey, J., and Ramjugernath, D.: Estimation of pure component properties, Fluid Phase Equilibria, 269, 117–133, https://doi.org/10.1016/j.fluid.2008.04.020, 2008.

Nenes, A., Pilinis, C., and Pandis., S. N.: ISORROPIA: A New Thermodynamic Model for Multiphase Multicomponent Inorganic Aerosols., Aquatic Geochemistry, 4, 123–152, 1998.

Palm, B. B., de Sá, S. S., Day, D. A., Campuzano-Jost, P., Hu, W., Seco, R., Sjostedt, S. J., Park, J.-H., Guenther, A. B., Kim, S., Brito, J., Wurm, F., Artaxo, P., Thalman, R., Wang, J., Yee, L. D., Wernis, R., Isaacman-VanWertz, G., Goldstein, A. H., Liu, Y., Springston, S. R., Souza, R., Newburn, M. K., Alexander, M. L., Martin, S. T., and Jimenez, J. L.: Secondary organic aerosol formation from ambient air in an oxidation flow reactor in central Amazonia, Atmospheric Chemistry and Physics, 18, 467–493, https://doi.org/10.5194/acp-18-467-2018, 2018.

Pankow, J. F.: An absorption model of gas/particle partitioning of organic compounds in the atmosphere, Atmospheric Environment, 28, 185–188, https://doi.org/10.1016/1352-2310(94)90093-0, 1994.

Pankow, J. F., Marks, M. C., Barsanti, K. C., Mahmud, A., Asher, W. E., Li, J., Ying, Q., Jathar, S. H., and Kleeman, M. J.: Molecular view modeling of atmospheric organic particulate matter: Incorporating molecular structure and co-condensation of water, Atmospheric Environment, 122, 400–408, https://doi.org/10.1016/j.atmosenv.2015.10.001, 2015.

Paulot, F., Crounse, J. D., Kjaergaard, H. G., Kürten, A., St Clair, J. M., Seinfeld, J. H., and Wennberg, P. O.: Unexpected epoxide formation in the gas-phase photooxidation of isoprene., Science, 325, 730–3, https://doi.org/10.1126/science.1172910, http://www.ncbi.nlm.nih.gov/pubmed/19661425, 2009.

Pratt, K. A., Fiddler, M. N., Shepson, P. B., Carlton, A. G., and Surratt, J. D.: Organosulfates in cloud water above the Ozarks' isoprene source region, Atmospheric Environment, 77, 231–238, https://doi.org/10.1016/j.atmosenv.2013.05.011, 2013.

Raes, F.: Entrainment of free tropospheric aerosols as a regulating mechanism for cloud condensation nuclei in the remote marine boundary layer, Journal of Geophysical Research, 100, 2893, https://doi.org/10.1029/94JD02832, 1995.

Raventos-Duran, T., Camredon, M., Valorso, R., Mouchel-Vallon, C., and Aumont, B.: Structure-activity relationships to estimate the effective Henry's law constants of organics of atmospheric interest, Atmospheric Chemistry and Physics, 10, 7643–7654, https://doi.org/10.5194/acp-10-7643-2010, 2010.

Renard, P., Siekmann, F., Salque, G., Demelas, C., Coulomb, B., Vassalo, L., Ravier, S., Temime-Roussel, B., Voisin, D., and Monod, A.: Aqueous-phase oligomerization of methyl vinyl ketone through photooxidation - Part 1: Aging processes of oligomers, Atmospheric Chemistry and Physics, 15, 21–35, https://doi.org/10.5194/acp-15-21-2015, 2015.

Riemer, N. and West, M.: Quantifying aerosol mixing state with entropy and diversity measures, Atmospheric Chemistry and Physics, 13, 11 423–11 439, https://doi.org/10.5194/acp-13-11423-2013, 2013.

Saunders, S. M., Jenkin, M. E., Derwent, R. G., and Pilling, M. J.: Protocol for the development of the Master Chemical Mechanism, MCM v3 (Part A): tropospheric degradation of non-aromatic volatile organic compounds, Atmospheric Chemistry and Physics, 3, 161–180, https://doi.org/10.5194/acp-3-161-2003, http://www.atmos-chem-phys.net/3/161/2003/, 2003.

Schmid, B., Tomlinson, J. M., Hubbe, J. M., Comstock, J. M., Mei, F., Chand, D., Pekour, M. S., Kluzek, C. D., Andrews, E., Biraud, S. C., and McFarquhar, G. M.: The DOE arm aerial facility, Bulletin of the American Meteorological Society, 95, 723–742, https://doi.org/10.1175/BAMS-D-13-00040.1, 2014.

Shilling, J. E., Pekour, M. S., Fortner, E. C., Artaxo, P., de Sá, S., Hubbe, J. M., Longo, K. M., Machado, L. A. T., Martin, S. T., Springston, S. R., Tomlinson, J., and Wang, J.: Aircraft observations of the chemical composition and aging of aerosol in the Manaus urban plume during GoAmazon 2014/5, Atmospheric Chemistry and Physics, 18, 10 773–10 797, https://doi.org/10.5194/acp-18-10773-2018, 2018.

Shrivastava, M., Zelenyuk, A., Imre, D., Easter, R., Beranek, J., Zaveri, R. A., and Fast, J.: Implications of low volatility SOA and gas-phase fragmentation reactions on SOA loadings and their spatial and temporal evolution in the atmosphere, Journal of Geophysical Research: Atmospheres, 118, 3328–3342, https://doi.org/10.1002/jgrd.50160, 2013.

Shrivastava, M., Easter, R. C., Liu, X., Zelenyuk, A., Singh, B., Zhang, K., Ma, P.-L., Chand, D., Ghan, S., Jimenez, J. L., Zhang, Q., Fast, J., Rasch, P. J., and Tiitta, P.: Global transformation and fate of SOA: Implications of low-volatility SOA and gas-phase fragmentation reactions, Journal of Geophysical Research: Atmospheres, 120, 4169–4195, https://doi.org/10.1002/2014JD022563, 2015.

Shrivastava, M., Andreae, M. O., Artaxo, P., Barbosa, H. M. J., Berg, L. K., Brito, J., Ching, J., Easter, R. C., Fan, J., Fast, J. D., Feng, Z., Fuentes, J. D., Glasius, M., Goldstein, A. H., Alves, E. G., Gomes, H., Gu, D., Guenther, A., Jathar, S. H., Kim, S., Liu, Y., Lou, S., Martin, S. T., McNeill, V. F., Medeiros, A., de Sá, S. S., Shilling, J. E., Springston, S. R., Souza, R. A. F., Thornton, J. A., Isaacman-VanWertz, G., Yee, L. D., Ynoue, R., Zaveri, R. A., Zelenyuk, A., and Zhao, C.: Urban pollution greatly enhances formation of natural aerosols over the Amazon rainforest, Nature Communications, 10, 1046, https://doi.org/10.1038/s41467-019-08909-4, 2019.

Sinha, V., Williams, J., Crowley, J. N., and Lelieveld, J.: The comparative reactivity method - A new tool to measure total OH Reactivity in ambient air, Atmospheric Chemistry and Physics, 8, 2213–2227, https://doi.org/10.5194/acp-8-2213-2008, 2008.

Szopa, S., Aumont, B., and Madronich, S.: Assessment of the reduction methods used to develop chemical schemes: building of a new chemical scheme for VOC oxidation suited to three-dimensional multiscale HOx-NOx-VOC chemistry simulations, Atmospheric Chemistry and Physics, 5, 2519–2538, https://doi.org/10.5194/acp-5-2519-2005, 2005.

Tennekes, H.: A Model for the Dynamics of the Inversion Above a Convective Boundary Layer, Journal of the Atmospheric Sciences, 30, 558–567, https://doi.org/10.1175/1520-0469(1973)030<0558:AMFTDO>2.0.CO;2, 1973.

Thalman, R., de Sá, S. S., Palm, B. B., Barbosa, H. M. J., Pöhlker, M. L., Alexander, M. L., Brito, J., Carbone, S., Castillo, P., Day, D. A., Kuang, C., Manzi, A., Ng, N. L., Sedlacek III, A. J., Souza, R., Springston, S., Watson, T., Pöhlker, C., Pöschl, U., Andreae, M. O., Artaxo, P., Jimenez, J. L., Martin, S. T., and Wang, J.: CCN activity and organic hygroscopicity of aerosols downwind of an urban region in central Amazonia: seasonal and diel variations and impact of anthropogenic emissions, Atmospheric Chemistry and Physics, 17, 11 779–11 801, https://doi.org/10.5194/acp-17-11779-2017, 2017.

Valorso, R., Aumont, B., Camredon, M., Raventos-Duran, T., Mouchel-Vallon, C., Ng, N. L., Seinfeld, J. H., Lee-Taylor, J., and Madronich, S.: Explicit modelling of SOA formation from $\alpha$-pinene photooxidation: sensitivity to vapour pressure estimation, Atmospheric Chemistry and Physics, 11, 6895–6910, https://doi.org/10.5194/acp-11-6895-2011, 2011.

Wang, Y., Hu, M., Guo, S., Wang, Y., Zheng, J., Yang, Y., Zhu, W., Tang, R., Li, X., Liu, Y., Le Breton, M., Du, Z., Shang, D., Wu, Y., Wu, Z., Song, Y., Lou, S., Hallquist, M., and Yu, J.: The secondary formation of organosulfates under interactions between biogenic emissions and anthropogenic pollutants in summer in Beijing, Atmospheric Chemistry and Physics, 18, 10 693–10 713, https://doi.org/10.5194/acp-18-10693-2018, 2018.

Wendisch, M., Poschl, U., Andreae, M. O., MacHado, L. A., Albrecht, R., Schlager, H., Rosenfeld, D., Martin, S. T., Abdelmonem, A., Afchine, A., Araujo, A. C., Artaxo, P., Aufmhoff, H., Barbosa, H. M., Borrmann, S., Braga, R., Buchholz, B., Cecchini, M. A., Costa, A., Curtius, J., Dollner, M., Dorf, M., Dreiling, V., Ebert, V., Ehrlich, A., Ewald, F., Fisch, G., Fix, A., Frank, F., Futterer, D., Heckl, C., Heidelberg, F., Huneke, T., Jakel, E., Jarvinen, E., Jurkat, T., Kanter, S., Kastner, U., Kenntner, M., Kesselmeier, J., Klimach, T., Knecht, M., Kohl, R., Kolling, T., Kramer, M., Kruger, M., Krisna, T. C., Lavric, J. V., Longo, K., Mahnke, C., Manzi, A. O., Mayer, B., Mertes, S., Minikin, A., Molleker, S., Munch, S., Nillius, B., Pfeilsticker, K., Pohlker, C., Roiger, A., Rose, D., Rosenow, D., Sauer, D., Schnaiter, M., Schneider, J., Schulz, C., De Souza, R. A., Spanu, A., Stock, P., Vila, D., Voigt, C., Walser, A., Walter, D., Weigel, R., Weinzierl, B., Werner, F., Yamasoe, M. A., Ziereis, H., Zinner, T., and Zoger, M.: Acridicon-chuva campaign: Studying tropical deep convective clouds and precipitation over amazonia using the New German research aircraft HALO, Bulletin of the American Meteorological Society, 97, 1885–1908, https://doi.org/10.1175/BAMS-D-14-00255.1, 2016.

Wesely, M. L.: Parametrization of surface resistance to gaseous dry deposition in regional-scale numerical model, Atmospheric Environment, 23, 1293–1304, 1989.

Worden, H. M., Bloom, A. A., Worden, J. R., Jiang, Z., Marais, E., Stavrakou, T., Gaubert, B., and Lacey, F.: New Constraints on Biogenic Emissions using Satellite-Based Estimates of Carbon Monoxide Fluxes, Atmospheric Chemistry and Physics Discussions, 30, 1–19, https://doi.org/10.5194/acp-2019-377, 2019.

Xu, L., Guo, H., Boyd, C. M., Klein, M., Bougiatioti, A., Cerully, K. M., Hite, J. R., Isaacman-VanWertz, G., Kreisberg, N. M., Knote, C., Olson, K., Koss, A., Goldstein, A. H., Hering, S. V., de Gouw, J., Baumann, K., Lee, S.-h., Nenes, A., Weber, R. J., and Ng, N. L.: Effects of anthropogenic emissions on aerosol formation from isoprene and monoterpenes in the southeastern United States, Proceedings of the National Academy of Sciences, 112, 37–42, https://doi.org/10.1073/pnas.1417609112, 2015.

Yee, L. D., Isaacman-VanWertz, G., Wernis, R. A., Meng, M., Rivera, V., Kreisberg, N. M., Hering, S. V., Bering, M. S., Glasius, M., Upshur, M. A., Bé, A. G., Thomson, R. J., Geiger, F. M., Offenberg, J. H., Lewandowski, M., Kourtchev, I., Kalberer, M., de Sá, S.,

https://doi.org/10.5194/acp-2019-1024
Preprint. Discussion started: 21 November 2019
© Author(s) 2019. CC BY 4.0 License.



Martin, S. T., Alexander, M. L., Palm, B. B., Hu, W., Campuzano-Jost, P., Day, D. A., Jimenez, J. L., Liu, Y., McKinney, K. A., Artaxo, P., Viegas, J., Manzi, A., Oliveira, M. B., de Souza, R., Machado, L. A. T., Longo, K., and Goldstein, A. H.: Observations of sesquiterpenes and their oxidation products in central Amazonia during the wet and dry seasons, Atmospheric Chemistry and Physics, pp. 1–31, https://doi.org/10.5194/acp-2018-191, 2018.

Zaveri, R. A., Easter, R. C., Fast, J. D., and Peters, L. K.: Model for Simulating Aerosol Interactions and Chemistry (MOSAIC), Journal of Geophysical Research, 113, 1–29, https://doi.org/10.1029/2007JD008782, 2008.

Zhao, Y., Nguyen, N. T., Presto, A. A., Hennigan, C. J., May, A. A., and Robinson, A. L.: Intermediate Volatility Organic Compound Emissions from On-Road Diesel Vehicles: Chemical Composition, Emission Factors, and Estimated Secondary Organic Aerosol Production, Environmental Science and Technology, 49, 11 516–11 526, https://doi.org/10.1021/acs.est.5b02841, 2015.

Zhao, Y., Nguyen, N. T., Presto, A. A., Hennigan, C. J., May, A. A., and Robinson, A. L.: Intermediate Volatility Organic Compound Emissions from On-Road Gasoline Vehicles and Small Off-Road Gasoline Engines, Environmental Science and Technology, 50, 4554–4563, https://doi.org/10.1021/acs.est.5b06247, 2016.